1. Report No.	2. Government Accession No.	3. Recipient's Catalog No.
NASA CR-132450		

4. Title and Subtitle	5. Report Date
COMOC: Three-Dimensional Boundary Region Variant, Theoretical Manual and User's Guide	May 1974
	6. Performing Organization Code
7. Author(s)	8. Performing Organization Report No.
A.J. Baker & S.W. Zelazny	D9192-950002
9. Performing Organization Name and Address	10. Work Unit No.
Bell Aerospace Company P.O. Box One Buffalo, New York 14240	11. Contract or Grant No. NAS1-11214
	13. Type of Report and Period Covered
12. Sponsoring Agency Name and Address	Contractor Report
National Aeronautics and Space Adm. Washington, D.C. 20546	14. Sponsoring Agency Code

15. Supplementary Notes

16. Abstract

The Three-Dimensional Boundary Region Variant of the COMOC computer program system solves the three-dimensional boundary region equations for a viscous, heat conducting, multiple species, compressible fluid including combustion. The governing partial differential equations are solved in physical variables. The flow may be subsonic or supersonic, laminar and/or turbulent, and may contain up to nine or more distinct species in frozen composition or undergoing equilibrium chemical reaction for a hydrogen/oxygen/air system. The program is equally applicable to computations in two- and three-dimensional boundary layer flows. COMOC is based upon a finite element solution algorithm for the partial differential equation systems. It employs a finite difference integration algorithm procedure to solve the resultant systems of first-order, ordinary differential equations. Boundary condition constraints on the normal flux and tangential distribution of each dependent variable are user-specifiable on arbitrarily disjoint segments of the solution domain closure. The solutions for each dependent variable, and all computed parameters, are established at node points lying on a specifiably non-regular computational lattice. The numerical solution establishes three-dimensional distributions of the three scalar velocity components, enthalpy, temperature, density, viscosity, and applicable species mass fractions. Variable Prandtl number and species diffusion coefficient distributions may be utilized. This report documents the theoretical and mechanical structure of the computer program, and presents guidance on adaptation of the code to solution of a particular problem. Sample solutions are discussed for several problems, especially with respect to solution accuracy and speed as a function of parameters under control of the user. Construction of input data decks for sample problems is discussed.

17. Key Words (Selected by Author(s))	18. Distribution Statement
Numerical Solution Three-Dimensional Flow Finite Element Algorithm Compressible, Turbulent Equilibrium Reacting	For U.S. Government Agencies and their Contractors only

19. Security Classif. (of this report)	20. Security Classif. (of this page)	21. No. of Pages	22. Price*
Unclassified	Unclassified	73	

*For sale by the Clearinghouse for Federal Scientific and Technical Information, Springfield, Virginia 22151.

Page Intentionally Left Blank

TABLE OF CONTENTS

ILLUSTRATIONS

TABLES

COMOC: THREE DIMENSIONAL BOUNDARY REGION VARIANT THEORETICAL MANUAL AND USER'S GUIDE

By

A. J. Baker & S. W. Zelazny

Bell Aerospace Company

SUMMARY

The Three-Dimensional Boundary Region Variant of the COMOC computer program system solves the three-dimensional boundary region equations for flow of a viscous, heat conducting, multiple species, compressible fluid including combustion. The governing partial differential equations are solved in physical variables, and allow complete two-dimensional diffusion in the plane transverse to the predominant direction of flow. The flow field may be external or confined, subsonic or supersonic, laminar and/or turbulent, and may contain up to nine or more distinct species in frozen composition or undergoing equilibrium chemical reaction for a hydrogen/oxygen/air system. The program is equally applicable to computations in two- and three-dimensional boundary layer flows wherein diffusion in only one direction is important.

The COMOC computer program is based upon a finite element solution algorithm for the elliptic partial differential operator in the parent equation system. It employs an explicit finite difference integration procedure to solve the resultant systems of first-order, ordinary differential equations. Boundary condition constraints on the normal flux and tangential distribution of each dependent variable are user-specifiable on arbitrarily disjoint segments of the solution domain closure. The solutions for each dependent variable, and all computed parameters, are established at node points lying on a specifiably non-regular computational lattice formed by plane triangulation of the solution domain. The numerical solution establishes the complete three-dimensional distributions of the three scalar velocity components, enthalpy, temperature, density, viscosity, and all applicable species mass fractions, as well as various integral flow parameters. Variable Prandtl number and species diffusion coefficient distributions may be utilized. Initial distributions of all dependent variables may be arbitrarily specified.

This report documents the theoretical and mechanical structure of the computer program, and presents detailed guidance on adaptation of the code to solution of a particular problem.

Sample solutions are discussed for several problems, especially with respect to solution accuracy and speed as a function of parameters under control of the user. Construction of the input data decks for sample problems is discussed. A programmer's manual has been separately published [Ref. 1].

INTRODUCTION AND USER GUIDELINES

The finite element methodology for numerical solution of initial-boundary value problems in continuum mechanics is undergoing an explosive rate of growth. Formerly considered to be constrained to solution of problems in structural analysis, or other linear field problems wherein an equivalent extremum principle exists, the theoretical support is now sufficiently generalized to render the method directly applicable to explicitly nonlinear problems, including the Navier-Stokes equations [Ref. 2-4]. The COMOC computer program system is being developed to transmit this rapid theoretical progress (often couched in intricate mathematical formalism) into a viable and versatile numerical solution capability. As such, it must be applicable to diverse and complex problems in computational continuum mechanics while requiring minimal mathematical prowess on the part of the user. On the way to generation of this general purpose concept, several Variants of COMOC have been developed for specific problem classes including transient thermal analysis [Ref. 5] and the two-dimensional Navier Stokes equations [Ref. 6]. This report documents the developed Three-Dimensional Boundary Region (3DBR) Variant of COMOC, and describes its applicability to a wide range of practical two- and three-dimensional flow problems.

The 3DBR Variant of COMOC solves the three-dimensional boundary region equations for flow of a viscous, heat conducting, multiple-species, compressible fluid including combustion. The governing partial differential equation system, developed in rectangular Cartesian coordinates from the parabolic Navier-Stokes equations, allows complete diffusion in the plane perpendicular to the uniformly discernible predominant flow direction. The flow may be external or confined, subsonic or supersonic, laminar and/or turbulent, and can contain up to nine or more distinct species in frozen composition or undergoing equilibrium chemical reaction for a hydrogen/oxygen/air system. The finite element solution procedure marches the discretized equivalent of the governing equation system in the direction parallel to the predominant flow. It numerically establishes the complete three-dimensional distributions of the three scalar velocity components, enthalpy, temperature, density, viscosity, and all applicable species mass fractions, as well as various integral flow parameters. No restrictions or simplifying assumptions are made for

the Prandtl number, and individual species diffusion coefficients are treated as variable parameters. Initial distributions of all dependent variables may be arbitrarily specified. Boundary condition constraints on the normal flux and tangential distribution of each dependent variable are user-specifiable on arbitrarily disjoint segments of the solution domain closure. The solutions for each dependent variable, and all computed parameters, are established at node points lying on a specifiably non-regular computational lattice formed by plane triangulation of the solution domain.

All Variants of the COMOC system are built upon the macrostructure illustrated in Fig. 1. The Main executive routine allocates core, using a variable dimensioning scheme, based upon the total degrees of freedom of the problem. The size of the largest problem that can be solved is thus limited (only) by the core size of the computer in use. The precise mix between number of dependent variables (and parameters), and fineness of the discretization, is user-specifiable and widely variable. The Input module serves its standard function for all dependent variable, parameter, and geometric coordinate arrays. The Discretization module forms the finite element discretization of the solution domain, and evaluates all required finite element non-standard matrices and standard-matrix multipliers. The Initialization module computes the remaining initial parametric data required to start the solution. The Integration Module constitutes the primary execution sequence of problem solution. It is based upon an integration algorithm for the column vector of unknowns of the solution, for which the discretized description is initial-valued. Calls to auxiliary routines for parameter evaluation, e.g. viscosity, Prandtl number, source terms, combustion parameters, etc., as specified functions of dependent and/or independent variables are governed by the Integration Module. The user has considerable latitude to adapt COMOC to the specifics of his particular problem at this point, by directly inserting easily written subroutines into COMOC to compute special forms of these parameters. The Output module is similarly addressed from the integration sequence and serves its standard function via a highly automated array display algorithm. COMOC can execute distinct problems in sequence and contains an automatic restart capability to continue solutions.

The 3DBR Variant of COMOC, as a direct consequence of the expansive problem class to which it may be addressed, is a fairly large and complex computer program. The vigor with which the potential user of a computer code attacks preparation of a data deck decreases exponentially (at least) with the thickness of the instruction manual. It is the intent of this user's guide to, in a minimum amount of space, present general guidelines for the use of COMOC, describe the rudiments of the differential equation system being solved, briefly expose the basic mathematics

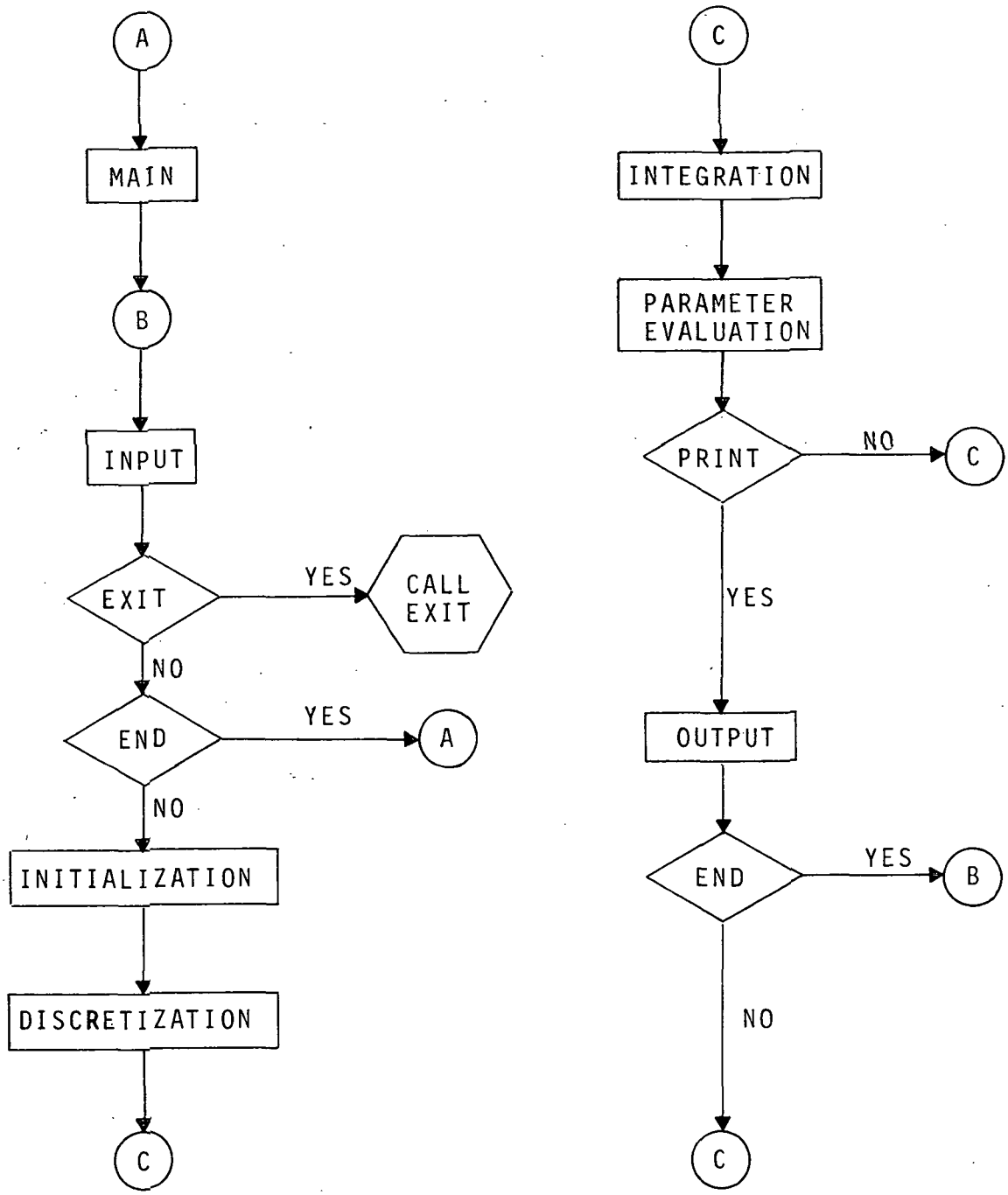

Figure 1. COMOC Macro-Structure

of the finite element algorithm and its numerical embodiment, and discuss sample solutions with respect to accuracy, solution, speed, and diversity. The standard test cases that accompany COMOC are discussed in terms of the physics of the solution as well as the description of data deck preparation. A large effort has been made to simplify and streamline data preparation and to require the user to specify an absolute minimum of non-physical or non-engineering input. The basic program contains a multitude of options which could potentially lead to confusion on the part of the user. Most of these have been suppressed, particularly in the output sub-program, with default instructions or values. The programmer's manual [Ref. 1] describes how they may be returned to an operational status.

The following general guidelines will assist the potential user on adapting 3DBR COMOC to a given problem.

Solution Domain Configuration

Most three-dimensional flow fields for which, 1) a predominant flow direction persists (i.e., no recirculation component), 2) a prescribed pressure gradient can be established, and 3) no imbedded shocks occur, are amenable to analysis using 3DBR COMOC. This includes two- and three-dimensional boundary layer flows, certain two- and three-dimensional flows in environmental hydrodynamics, and free-, slot-, and boundary-jet injection configurations typical of combustors. Boundary conditions can be applied to the entire solution domain closure with local normal orthogonal to the direction of predominant flow. An initial distribution (including zero) of all dependent variables is needed to start the solution. However, a downstream outflow boundary condition is specifically not required.

Variables and Parameters

The computational variables are the three scalar components of velocity, stagnation enthalpy, and mass fraction of all identifiable species. Perfect gas behavior is assumed. The present 3DBR Variant solves the mainstream and one cross-plane velocity component as a boundary value problem; it employs the continuity equation to establish the remaining cross-plane velocity component. The program computes static temperature and density, and all thermophysical properties may be temperature and mass fraction dependent. Unless overridden by a user provided subroutine, viscosity is computed from Sutherland's law. The Prandtl and Schmidt numbers may be variable. Equilibrium combustion of arbitrary mixtures of hydrogen, oxygen, and air can be established including local heat release and formation of NO. In the absence of diluents, this capability provides equilibrium gas behavior for air computations including dissociation.

Discretization

The nature of the flows to which this Variant is applicable yields the requirement for two-dimensional finite element discretizations only. Since the continuity equation is employed to solve for a transverse velocity component, it is advantageous to have node columns oriented parallel to that coordinate. This requirement for grid regularity has been built into an automatic discretizer for 3DBR COMOC. Considering flow in an axial corner for example, see Fig. 2, it might be desired to use a finer grid near the walls where larger dependent variable gradients would exist. The user need specify (only) the desired incremental spacing between node columns and rows. The discretizer will automatically triangulate the domain on these node point coordinates, and prepare the required geometric input data. This discretizer is not directly applicable to non-rectangular domains; however, 3DBR COMOC can accept discretizations formed manually or from other automated sources.

Boundary Conditions

Constraints can be imposed on the admissible behavior of each dependent variable and its normal flux, i.e., gradient, on all surfaces bounding the solution domain, see Fig. 2. These surfaces may constitute actual physical boundaries of the problem or be strictly mathematical. As an example of the latter, employing symmetry planes to enclose a solution domain is particularly advantageous in terms of computer execution time and user input effort. The attendant vanishing gradient constraint is the automatic default value within the finite element solution algorithm, and its use does not require generation of any phantom cells or special node handling. Fixing the normal gradient in terms of the dependent variable is equally straightforward, and is useful for thermally porous walls or a slip wall boundary condition. Here again, no special cells or node handling is required on the part of the user.

Input Preparation

A concerted effort has been made to render input preparation minimal and in terms of physically meaningful variables and expressions. However, should the solution to a dozen or more dependent variables be sought, the input deck can become of substantial size. The program accepts input in the English system of units; it outputs non-dimensionalizing constants and solution parameters in several systems, and provides detailed output arrays of computed non-dimensional dependent variables. The program executes under automatic error control and will adjust integration step-size to maintain an accurate and stable solution. The only user input required for this phase is the initial and final

integration stations and the desired interval for output. Some additional options exist that can speed execution for some cases [Ref. 1]. These parameters are defaulted to "best" values if not overridden by the user.

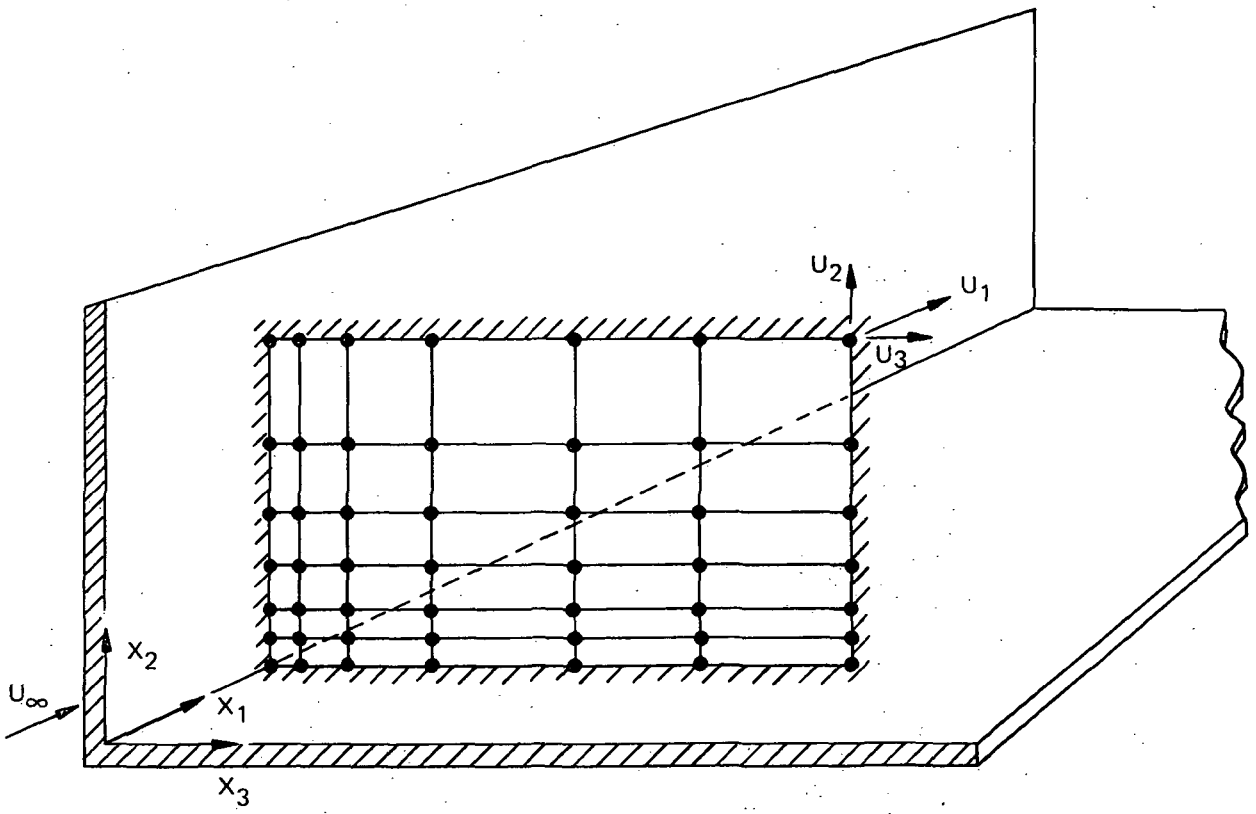

Figure 2. Illustrative Finite Element Discretization

User-Written Subroutines

COMOC provides the user with considerable latitude for appending subroutines to perform specific parameter computations. Included in this category are pressure gradient, laminar and/or turbulent viscosity, and Prandtl and Schmidt numbers. In all cases, a skeletal subroutine is filled in by the user to include an equation or tabular data of the parametric dependence on any number of independent or dependent variables in any combination. These subroutines are always written in terms of physical variables with dimensions consistent with the input data. Non-dimensionalization and calling sequence are controlled internally, and the user can obtain complete arrays of these computations from the output package.

Output

The 3DBR COMOC program contains a highly adaptive output subprogram. The user has considerable latitude in specifying output arrangements, both dimensional and non-dimensional, from the input deck. The output routine is adapted to compute integral flow parameters including wall shear, Stanton number, and mixing efficiency. Data sets are automatically scaled and ordered to be geometrically similar to the physical problem for all discretizations, both regular and non-regular.

Computational Costs

The computer cost associated with generating a COMOC solution to a given problem can be approximately estimated. CPU costs are basically a function of the number of dependent variables in the solution, the amount of output requested, out-of-core operations associated with restart and/or plot tape preparation, and the thermodynamics of the solution. The use of rather course discretizations is strongly recommended for initial evaluation of any problem. Employing progressively finer discretizations will generally improve solution accuracy with a more-than-proportional increase in computational cost.

NOMENCLATURE

a	boundary condition coefficient
A	species; one-dimensional matrix; area
Ar	argon
b	coefficient
B	species; two-dimensional matrix
c	coefficient
c_p	specific heat
C	species; three-dimensional matrix
C_f	skin friction
d	differential
D	determinant
f	function of known argument

g	function of known argument
h	static enthalpy; integration step-size; stream depth
H	stagnation enthalpy; hydrogen
i	index
I	mass defect
$\hat{i},\hat{j},\hat{k}$	basis vectors of rectangular coordinate system
j	summation index; coefficient
J	Jacobian
k	thermal conductivity; integration stage number; constant
K	generalized diffusion coefficient; equilibrium constant
ℓ	differential operator; number; length
L	characteristic length; differential operator
m	number
M	Mach Number; number of finite elements
n	unit normal vector; number, nodes per element; dimensionality
N	nitrogen; composition matrix
O	oxygen
p	pressure; predicted value
Pr	Prandtl Number
q	generalized dependent variable
Q	generalized discretized dependent variable
r	position vector
R	domain of elliptic operator; universal gas constant
Re	Reynolds Number
S	mass source term; enthalpy boundary condition parameter

Sc	Schmidt Number
T	temperature
u,U	velocity
W	molecular weight
x_i	rectangular Cartesian coordinate system
X	species mole fraction
Y	species mass fraction
α	direction cosine
β	coefficient; pressure gradient parameter
γ	ratio of specific heats; turbulence intermittency factor
∂R	closure of solution domain
δ	boundary layer thickness
Δ	increment
ε	kinematic eddy viscosity; basis vectors; integration parameter
κ	coefficient
λ	multiplier
ξ	non-dimensional length
μ	viscosity
ρ	density
σ	integral kernel
τ	integral kernel; wall shear
ϕ,Φ	functional
χ	domain of initial value operator
ω	turbulence damping factor
Ω	global solution domain

{ }	column matrix
[ ]	square matrix
$\cup$	union
$\cap$	intersection
$\sum$	summation

Superscripts and Subscripts

*	approximate solution; reference state
′	derivative in the x_1 direction; transformation
T	matrix transpose
^	unit vector
~	reference state
-	constrained to solution domain closure
e	effective value; local reference condition
i,j,k,ℓ	tensor indices
m	pertaining to m^{th} subdomain (finite element)
n	integration stage
o	initial condition
x	evaluated at x_1
∞	global reference condition
α	species identification
β	elemental species identification

FINITE ELEMENT SOLUTION ALGORITHM FOR THE THREE-DIMENSIONAL BOUNDARY REGION EQUATIONS

The system of partial differential equations governing the three-dimensional boundary region flow of a compressible fluid is obtained from the parabolic approximation to the full Navier-Stokes equations. The parabolic approximation, i.e., "parabolic Navier-Stokes equations," describe steady, three-dimensional flows wherein, 1) a predominant flow direction is uniformly discernible, 2) in this direction (only), diffusion processes are negligible compared to convection, and 3) no disturbances are propagated upstream antiparallel to this direction. The boundary region equation system is obtained from parabolic Navier-Stokes with the single additional assumption that a known pressure distribution is superimposed upon the flow field. Conversely, the approximation may be viewed as generalization of the three-dimensional boundary layer equations to include diffusion processes in the complete two-dimensional plane of crossflow. Closure of this equation system requires identification of constitutive behavior. By employing an eddy coefficient hypothesis, the time-averaged turbulent flow equations appear identical to the laminar flow equations. Hence, the finite element development assumes a generalized transport coefficient description, distributed as laminar or turbulent at nodes of the discretization by the user.

The Three-Dimensional Boundary Region Equations

In three-dimensional space, spanned by a rectangular Cartesian coordinate system, identify the velocity vector

$$u_i \equiv u_1\hat{i} + u_2\hat{j} + u_3\hat{k} \tag{1}$$

For development of the differential equation system, assume that $\hat{i}$ is aligned parallel to the predominant flow direction. Identify a two-dimensional vector differential operator as

$$(\ )_{,k} \equiv \hat{j}(\ )_{,2} + \hat{k}(\ )_{,3} \tag{2}$$

where the comma identifies the gradient operator. Employing Cartesian tensor notation, with summation over 2 and 3 for repeated latin subscripts, the three-dimensional boundary region equation system for a multiple-species, compressible, reacting flow takes the form

$$0 = (\rho u_i)_{,i} + (\rho u_1)_{,1} \tag{3}$$

$$\rho u_1 Y^\alpha_{,1} = \left[\frac{\mu^e}{Sc \cdot Re} Y^\alpha_{,k}\right]_{,k} - \rho u_k Y^\alpha_{,k} + S^\alpha \tag{4}$$

$$\rho u_1 u_{1,1} = \left[\frac{\mu^e}{Re} u_{1,k}\right]_{,k} - \rho u_k u_{1,k} - p_{,1} \tag{5}$$

$$\rho u_1 u_{3,1} = \left[\frac{\mu^e}{Re} u_{3,k}\right]_{,k} - \rho u_k u_{3,k} - p_{,3} \tag{6}$$

$$\begin{aligned} \rho u_1 H_{,1} = & \left[\frac{\mu^e}{Re \cdot Pr} H_{,k}\right]_{,k} - \rho u_k H_{,k} \\ & - M_\infty^2 \left[\frac{1-Pr}{Pr} \frac{\mu^e}{2Re} (u_j u_j)_{,k}\right]_{,k} \\ & - \left[\frac{Sc-Pr}{Sc \cdot Pr} \frac{\mu^e}{Re} \sum_\alpha h^\alpha Y^\alpha_{,k}\right]_{,k} \end{aligned} \tag{7}$$

The variables appearing in Eq. (3)-(7) are non-dimensionalized with respect to ρ_∞, U_∞, c_{p_∞}, T_∞, and a length constant L, and have their usual interpretation in fluid mechanics. The Reynolds (Re), Prandtl (Pr), and Schmidt (Sc) numbers are defined with respect to the effective diffusion coefficient, μ^e, in algebraic combination with the laminar and turbulent contributions as, for example

$$\frac{\mu^e}{Pr} \equiv \frac{\mu}{Pr} + \frac{\rho\varepsilon}{Pr_T} \tag{8}$$

In Eq. (8), μ is the laminar viscosity, ε is the kinematic eddy viscosity, and subscript T denotes a turbulent reference parameter. The stagnation enthalpy is defined in terms of species static enthalpies as

$$H \equiv \sum_\alpha h^\alpha Y^\alpha + \frac{1}{2} u_k u_k \tag{9}$$

The static enthalpy includes the heat of formation, h^α_o, of the species in its definition as

$$h^\alpha \equiv \int_{T_o}^{T} c_p^\alpha dT + h_o^\alpha \tag{10}$$

An equation of state is required to close the system. Assuming perfect gas behavior for each species, from Dalton's law, obtain

$$p = \rho RT \sum_{\alpha} \frac{Y^{\alpha}}{W^{\alpha}} \tag{11}$$

where R is the universal gas constant and W^{α} is the molecular weight of the α-th species.

Equilibrium combustion of hydrogen/oxygen/air systems in three-dimensional boundary region flow is operational in 3DBR COMOC. The following reactions are assumed operative.

$$\begin{aligned} 2H + O &\rightleftarrows H_2O \\ 2H &\rightleftarrows H_2 \\ 2O &\rightleftarrows O_2 \\ H + O &\rightleftarrows OH \\ N_2 + 2O &\rightleftarrows 2NO \end{aligned} \tag{12}$$

The equilibrium composition of the combustion by-products is determined by applying the Law of Mass Action [Ref. 7] to each reaction defined in Eq. (12). This yields definition of a set of equilibrium rate constants, K, which, for the simple reaction $nA + mB \rightleftarrows \ell C$, are expressed in terms of species mole fraction, X^{α}, as

$$K \equiv \frac{[X^A]^n [X^B]^m}{[X^C]^{\ell}} \tag{13}$$

Solution of Eq. (12) with (13), and coupled with conservation of total and elemental mass, yields an algebraic equation system for determination of the equilibrium composition of the system, of the form.

$$[N_{\alpha}^{\beta}]\{X^{\alpha}\} = \{\text{const.}\} \tag{14}$$

In Eq. (14), the elements of the matrix $[N_{\alpha}^{\beta}]$ account for the particular species mole fraction distribution, $\{X^{\alpha}\}$, containing the β^{th} elemental material, e.g., O, H, and N.

Finite Element Solution Algorithm

The three-dimensional boundary region equation system, except for global continuity, Eq. (3), is uniformly an initial-boundary value problem of mathematical physics. Each of the partial differential equations, Eq. (4)-(7), is a special case of the general second-order, nonlinear partial differential equation

$$L(q) \equiv \kappa[K(q)q_{,k}]_{,k} + f(q,q_{,i},x_i) - g(q,\chi) = 0 \quad (15)$$

where q is a generalized dependent variable identifiable with each computational dependent variable. In Eq. (15), f and g are specified functions of their arguments, χ is identified with x_1 for boundary region flows, and x_i are the coordinates for which second order derivatives exist in the lead term. The finite element solution algorithm is based upon the assumption that L(q) is uniformly parabolic within a bounded open domain Ω, i.e., the lead term in Eq. (15) is uniformly elliptic within its domain R, with closure ∂R, where

$$\Omega = R \times [\chi_o,\chi) \quad (16)$$

and $\chi_o \leq \chi < \infty$. Table 1 lists the functions f and g, as well as the appropriate parameters, for Eq. (15) identified with each dependent variable.

For Eq. (15) uniformly parabolic, unique solutions for q are obtained pending specification of boundary constraints on ∂R and an initial condition on $R \cup \partial R$. For the former, the general form relates the function and its normal derivative everywhere on the closure, ∂R, as

$$\ell(q) \equiv a^{(1)}q(\bar{x}_i,\chi) + a^{(2)}Kq(\bar{x}_i,\chi),_k n_k - a^{(3)} = 0 \quad (17)$$

In Eq. (17), the $a^{(i)}(\bar{x}_i,\chi)$ are user-specified coefficients, see Table 2, the superscript bar notation constrains x_i to ∂R, and n_k is the local outward-pointing unit normal vector. For an initial distribution, assume given throughout $R \cup \partial R \times \chi_o$,

$$q(x_i,\chi_o) \equiv q_o(x_i) \quad (18)$$

TABLE 1

COEFFICIENTS IN GENERALIZED DIFFERENTIAL EQUATION

Eq. No.	q	κ	K	f	g
(4)	Y^{α}	Re^{-1}	$\frac{\mu^e}{Sc}$	$-\rho u_k Y^{\alpha}_{,k} + S^{\alpha}$	$\rho u_1 Y^{\alpha}_{,1}$
(5) & (6)	u_j	Re^{-1}	μ^e	$-\rho u_k u_{j,k} - p_{,j}$	$\rho u_1 u_{j,1}$
(7)	H	Re^{-1}	$\frac{\mu^e}{Pr}$	$-\rho u_k H_{,k} - M_\infty^2 \left[\frac{1-Pr}{Pr} \frac{\mu^e}{2Re} (u_j u_j)_{,k}\right]_{,k}$ $- \left[\frac{Sc-Pr}{ScPr} \frac{\mu^e}{Re} \sum_{\alpha} h^{\alpha} Y^{\alpha}_{,k}\right]_{,k}$	$\rho u_1 H_{,1}$

TABLE 2

GENERAL BOUNDARY CONDITION STATEMENT

Boundary Conditions	$a^{(1)}$	$a^{(2)}$	$a^{(3)}$
No Slip at Wall	1	0	0
Slip at Wall	+	1	0
Mass Injection	0	1	+
Adiabatic Wall	0	1	0
Specified Heat Flux	0	1	+
Temperature Dependent Flux	+	1	+
Symmetry Condition	0	1	0

+ User specified as non-zero to enforce desired condition level.

Formation of the finite element solution is obtained by establishing the algorithm for the equation system (15)-(18). Straightforward theoretical development is provided by using the Method of Weighted Residuals (MWR) formulated on a local basis. Since Eq. (15) is valid throughout R, it is valid within disjoint interior subdomains, R_m, described by $(x_i,\chi)\varepsilon R_m \times [\chi_o,\chi)$ called "finite elements," wherein $\cup R_m = R$. Form an approximate solution for q within $R_m \times [\chi_o,\chi)$, called $q_m^*(x_i,\chi)$, by expansion into a series solution of the form

$$q_m^*(x_i,\chi) \equiv \{\phi(x_i)\}^T\{Q(\chi)\}_m \qquad (19)$$

wherein the functionals $\phi_k(x_i)$ are members of a function set complete in R_m, and the unknown expansion coefficients, $Q_k(\chi)$, represent the χ-dependent values of $q_m^*(x_i,\chi)$ at specific locations interior to R_m and on the closure, ∂R_m, called "nodes." Equation (19) is a scalar, and selection of the particular ϕ_k is distinctly specifiable [Ref. 8] and can be problem class dependent.

To establish the values taken by the expansion coefficients in Eq. (19), require that the local error in the approximate solution to both the differential equation, $L(q_m^*)$, and the boundary condition statement, $\ell(q_m^*)$, for $\partial R_m \cap \partial R$, be rendered orthogonal to the space of the approximation functions. Employing an unknown algebraic multiplier, λ, the resultant equation sets can be combined as

$$\int_{R_m}\{\phi(x_i)\}L(q_m^*)d\tau - \lambda\int_{\partial R_m\cap\partial R}\{\phi(x_i)\}\ell(q_m^*)d\sigma \equiv 0 \qquad (20)$$

The number of equations (20) is identical to the number of node points of the finite element, R_m, i.e., the number of elements, n, in the column matrix, $\{Q(\chi)\}_m$, Eq. (19).

Equation (20) forms the basic operation of the finite element solution. Establishment of the global solution algorithm, and determination of λ, is accomplished by evaluating Eq. (20) in each of the M finite elements of the discretized solution domain, and assembly of these M × n equations into a global matrix system using Boolean algebra. The rank of the global system is less than M × n by connectivity of the finite element domains as well as boundary condition constraints on ∂R where $a^{(2)}$, Eq. (17), vanishes identically. The lead term in Eq. (15) can be rearranged, using the Green-Gauss Theorem, to yield

$$\int_{R_m} \{\phi(x_i)\}\kappa[Kq^*_m{}_{,k}]_{,k}\, d\tau = \kappa \oint_{\partial R_m} \{\phi(x_i)\} Kq^*_m{}_{,k} n_k\, d\sigma$$

$$- \kappa \int_{R_m} \{\phi(x_i)\}_{,k} Kq^*_m{}_{,k}\, d\tau \qquad (21)$$

For $\partial R \cap \partial R_m$ nonvanishing, Eq. (21), the corresponding segment of the closed surface integral will cancel the boundary condition contribution, Eq. (20), by identifying $\lambda a^{(2)}$ with κ of Eq. (15). The contributions to the closed surface integral, Eq. (21), where $\partial R_m \cap \partial R = 0$ can be made to vanish [Ref. 4]. Hence, combining Eq. (17)-(21), the globally assembled finite element solution algorithm for the representative partial differential equation system description becomes

$$\cup \left[- \kappa \int_{R_m} \{\phi\}_{,k} Kq^*_m{}_{,k}\, d\tau + \int_{R_m} \{\phi\}(f^*_m - g^*_m)\, d\tau \right.$$

$$\left. - \kappa \int_{\partial R_m \cap \partial R} \{\phi\}\left(a^{(1)}_m q^*_m - a^{(3)}_m\right) d\sigma \right] = \{0\} \qquad (22)$$

The rank of the global equation system, Eq. (22), is identical to the total number of node points on $R \cup \partial R$ for which the dependent variable requires solution. Equation (22) is a first-order, ordinary differential system, and the matrix structure is sparse and banded. Bandwidth is a function of both selected discretization and the order of the employed approximation functional, $\{\phi\}$, Eq. (19). Solution of the ordinary differential equation system is obtained using a finite difference numerical integration procedure.

A finite element solution algorithm for the global continuity equation is similarly derived. Recognizing that Eq. (3) is an initial value problem on ρu_2 as a function of x_2, with x_1 and x_3 appearing as parameters, the approximation function need span only the transverse coordinate direction as

$$q_m^* = \{\phi(x_2)\}^T \{Q(x_1, x_3)\}_m \tag{23}$$

The matrix elements Q_k are nodal values of ρu_2^*; their functional dependence requires solution of Eq. (3) along lines (x_1, x_3) equal a constant. The solution algorithm for Eq. (3) is directly specified as

$$\int_{R_m} \{\Phi\} L(\rho u_2^*) d\sigma = 0 \tag{24}$$

where the matrix elements of $\{\Phi\}$ need not be coincidental with those of $\{\phi\}$, Eq. (23), and the segments R_m correspond to lines of (x_1, x_3) equal to a constant.

THE THREE-DIMENSIONAL BOUNDARY REGION VARIANT OF COMOC

The COMOC computer program system has been established to embody the finite element solution algorithm for systems of equations, Eq. (15)-(18). The computer program evaluates Eq. (22) for each of the appropriate dependent variables, Table 1, including up to nine or more species mass fractions, marches the resultant ordinary differential equation system downstream, and includes a continuity equation solver for Eq. (24). This section presents the theoretical aspects of these solution techniques as embodied in the 3DBR Variant of COMOC.

Finite Element Matrix Generation

The fundamental finite element operation is formation of Eq. (22) on R_m and ∂R_m. The 3DBR Variant universally employs linear approximation functions, Eq. (19), for all dependent variables. The intrinsic finite element shapes for one- and two-dimensional space spanned by simplex functionals, are the line and triangle, Fig. 3. Accurate determination of the element matrices of Eq. (22) is mandatory, and involves evaluation of various-order moment distributions over the domain and on the closure of the finite element. Natural coordinate functionals, adapted from the area coordinates of structural mechanics [Ref. 8], are utilized. Simplex functionals are a linearly dependent set of normalized functions that are orthogonal to the respective closure segments of the finite element domain. For an n-dimensional space, there are n + 1 simplex natural coordinate functions. Table 3 contains the implicit definition of these functions in their respective spaces. The natural coordinate functions vanish at all node points of the finite element except one where the value is unity; hence, these functions are the elements of the approximation functional matrix, $\{\phi\}$, Eq. (19). Integration of arbitrary-order products of scalar elements of the $\{\phi\}$, over the domain of the finite element, are analytically evaluated in terms of the exponent distribution, see Table 4. For the present case, the equation system descriptions require moment generation in Euclidean space spanned by a rectangular Cartesian basis. All computations are performed in the local (primed) coordinate system, Fig. 3, defined by the tensor transformation law

$$x'_i = \alpha_{ij} x_j + r_i \qquad (25)$$

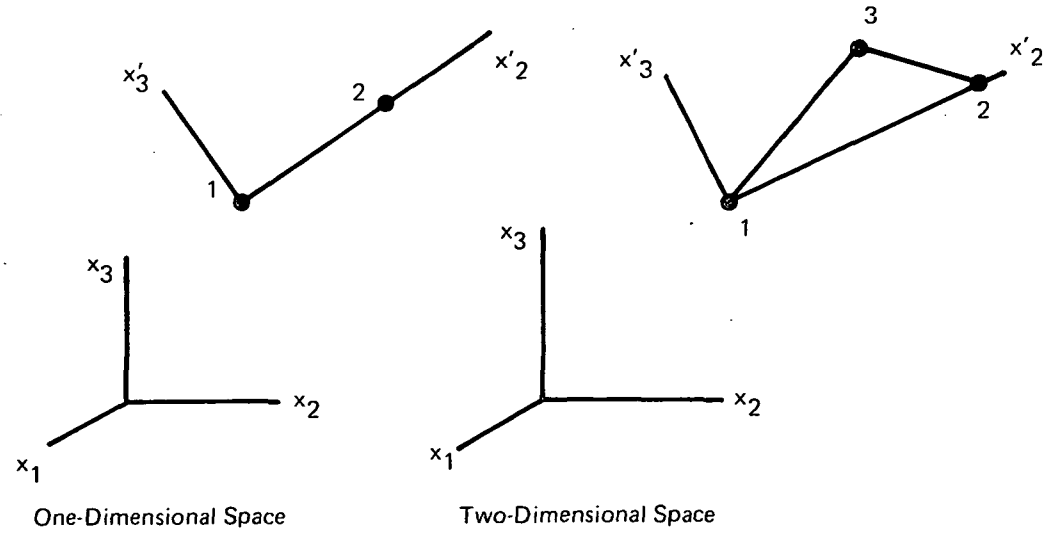

Figure 3. Intrinsic Finite Element Domains for Simplex Approximation Functions

TABLE 3

IMPLICIT DEFINITION OF SIMPLEX NATURAL COORDINATE FUNCTIONS

Dimensions	Element	Nodes	Natural Coordinate Definition
1	Line	2	$\begin{bmatrix} 1 & 1 \\ x_1^1 & x_1^2 \end{bmatrix} \begin{Bmatrix} \phi_1 \\ \phi_2 \end{Bmatrix} = \begin{Bmatrix} 1 \\ x_1 \end{Bmatrix}$
2	Triangle	3	$\begin{bmatrix} 1 & 1 & 1 \\ x_1^1 & x_1^2 & x_1^3 \\ x_2^1 & x_2^2 & x_2^3 \end{bmatrix} \begin{Bmatrix} \phi_1 \\ \phi_2 \\ \phi_3 \end{Bmatrix} = \begin{Bmatrix} 1 \\ x_1 \\ x_2 \end{Bmatrix}$

TABLE 4

INTEGRALS OF NATURAL COORDINATE FUNCTION PRODUCTS OVER FINITE ELEMENT DOMAINS

Dimensions	Integrals*
1	$\int_R \phi_1^{n_1} \phi_2^{n_2} \, d\sigma = D \frac{n_1! n_2!}{(n+n_1+n_2)!}$
2	$\int_R \phi_1^{n_1} \phi_2^{n_2} \phi_3^{n_3} \, d\tau = D \frac{n_1! n_2! n_3!}{(n+n_1+n_2+n_3)!}$

* D = Determinant of coefficient matrix defining the natural coordinate system, see Table 3.

n = Dimensionality of the finite element space

where r_i is the position vector to the origin of the primed coordinate system, and the α_{ij} are the direction cosines of the coordinate transformation. The integration kernels for two-dimensional space, Eq. (22), are

$$d\tau = dx_2' dx_3' \tag{26}$$

$$d\sigma = dx_2' \tag{27}$$

The first term in Eq. (22) is standard for all dependent variables. Assuming the generalized diffusion coefficient is distributed over the m^{th} element as a dependent variable, obtain

$$\kappa\int_{R_m}\{\phi\}_{,k}Kq^*_{m,k}d\tau = \kappa\int_{R_m}\{\phi\}_{,k}\{K\}^T_m\{\phi\}\{\phi\}^T_{,k}\{Q\}d\tau$$

$$= \kappa\{K\}^T_m\{B10\}[B211S]\{Q\}_m \qquad (28)$$

In Eq. (28) and the following, matrices with B prefixes are standard two-dimensional forms defined in Table 5. For Eq. (22) identified with each dependent variable, f^*_m and g^*_m universally contain the nonlinear convection term and the initial-value operator as dominant terms. The finite element equivalent for convection is

$$\int_{R_m}\{\phi\}\rho u^*_k q^*_{;k}d\tau = \int_{R_m}\{\phi\}\{\phi\}^T\{\rho u'_k\}_m\{\phi\}^T_{,k}\{Q\}_m d\tau$$

$$= [B200S]\{\rho U'\}_m\{B11\}^T\{Q\}_m \qquad (29)$$

where the elements of the vector, $\{\rho u'_k\}$, are nodal values of the planar mass flux transformed to the local coordinate systems via

$$u'_k = \alpha_{kj}u_j \qquad (30)$$

The initial-value operator, which comprises the mainstream convection term, similarly becomes

$$\int_{R_m}\{\phi\}\rho u^*_1 q^*_{;1}d\tau = \int_{R_m}\{\phi\}\{\phi\}^T\{\rho U1\}_m\{L\}^T\{Q\}'_m d\tau$$

$$= \{\rho U1\}^T_m[B3000S]\{Q\}'_m \qquad (31)$$

where the matrix elements of [B3000S] are column matrices, see Table 5. The superscript prime exterior to a matrix denotes an ordinary derivative.

TABLE 5

STANDARD FINITE ELEMENT MATRIX FORMS FOR SIMPLEX FUNCTIONALS IN ONE- AND TWO-DIMENSIONAL SPACE

Matrix[1] Name	Matrix Function	Matrix Evaluation[2],[3],[4]
{B10}	$\int_{R_m} \{\phi\} d\tau$	$\frac{A^m}{3}\begin{Bmatrix}1\\1\\1\end{Bmatrix}$
[B211S]	$\{\phi\}_{,k}\{\phi\}^T_{,k}$	$\left(\frac{1}{X2P2}\right)^2\begin{bmatrix}1 & -1 & 0\\ & 1 & 0\\ & & 0\end{bmatrix}$ $+\left(\frac{1}{X3P3}\right)^2\begin{bmatrix}\left(\frac{X3P3}{X2P2}-1\right)^2 & \frac{X3P3}{X2P2}\left(\frac{X3P3}{X2P2}-1\right) & -\left(\frac{X3P3}{X2P2}-1\right)\\ & \left(\frac{X3P3}{X2P2}\right)^2 & -\left(\frac{X3P3}{X2P2}\right)\\ & & 1\end{bmatrix}$
[B200S]	$\int_{R_m} \{\phi\}\{\phi\}^T d\sigma$	$\frac{A^m}{12}\begin{bmatrix}2 & 1 & 1\\ & 2 & 1\\ & & 2\end{bmatrix}$
[B3000S]	$\int_{R_m} \{\phi\}\{\phi\}\{\phi\}^T d\tau$	$\frac{A^m}{60}\begin{bmatrix}\begin{Bmatrix}6\\2\\2\end{Bmatrix} & \begin{Bmatrix}2\\2\\1\end{Bmatrix} & \begin{Bmatrix}2\\1\\2\end{Bmatrix}\\ & \begin{Bmatrix}2\\6\\2\end{Bmatrix} & \begin{Bmatrix}1\\2\\2\end{Bmatrix}\\ & & \begin{Bmatrix}2\\2\\6\end{Bmatrix}\end{bmatrix}$
{B11}	$\{\phi\}_{,k}$	$\hat{\epsilon}_2 \cdot \begin{Bmatrix}\phi_1\\\phi_2\\\phi_3\end{Bmatrix}_{,2} + \hat{\epsilon}_3 \cdot \begin{Bmatrix}\phi_1\\\phi_2\\\phi_3\end{Bmatrix}_{,3}$
[A200S]	$\int_{\partial R_m} \{\phi\}\{\phi\}^T d\sigma$	$\frac{\ell^m}{6}\begin{bmatrix}2 & 1\\ & 2\end{bmatrix}$
{A10}	$\int_{\partial R_m} \{\phi\} d\sigma$	$\frac{\ell^m}{2}\begin{Bmatrix}1\\1\end{Bmatrix}$

(1) Matrix names are a 6 digit code covering dimensionality, nonlinearity, degree of differentiation and special matrix properties, as [a, b, c, d, e, f] where:
a = A, B, C for spaces of one-, two-, and three-dimensions,
b = number of coordinate functions appearing in integral or matrix,
c, d, e = (0,1) Boolean counters indicating (no, yes) differentiation of each function,
e or f = S, A, Δ for matrix symmetric, antisymmetric or general.

(2) Symmetric matrices are written in upper triangular form.

(3) A^m = 1/2 (X2P2)(X3P3), the plane area of the triangular finite element.
X2P2 = the x_2 prime coordinate of node 2,
X3P3 = the x_3 prime coordinate of node 3.

(4) ℓ^m = length of side for boundary condition (=X2P2).

Both momentum Eq. (5) and (6) contain contributions to f_m^* stemming from a specified pressure distribution. For the mainstream momentum equation, a specified longitudinal pressure gradient, $p_{,1}$, is assumed known; hence,

$$\int_{R_m} \{\phi\} p_{,1} d\tau = \{B10\} p_{,1}(x_1) \tag{32}$$

For a lateral pressure gradient, obtain

$$\int_{R_m} \{\phi\} p_{,3} d\tau = \int \{\phi\}\{\phi\}^T_{,3} \{PZ\}_m d\tau = \{B10\}\{B11\}^T \{PZ\}_m \tag{33}$$

where the matrix elements of $\{PZ\}_m$ are obtained from the tensor transformation law, Eq. (25), as

$$PZ_k = \alpha_{k3} p_{,3} \tag{34}$$

Each species continuity equation, Eq. (4), may have a source term. Assuming the distribution to lie over the nodes of the discretization, obtain

$$\int_{R_m} \{\phi\} S^\alpha d\tau = \int_{R_m} \{\phi\}\{\phi\}^T \{S^\alpha\}_m d\tau = [B200S]\{S^\alpha\}_m \tag{35}$$

For non-constant Prandtl and Schmidt Numbers, the energy equation, Eq. (7), has two source terms. An integration using a Green-Gauss Theorem is appropriate for both; the generated surface integrals vanish by pairs on interior ∂R_m and are identically zero on $\partial R_m \cap \partial R$ for non-slip, non-porous walls. For the first term, Table 1, obtain

$$\int_{R_m} \{\phi\} \left[\frac{M_\infty^2}{2Re} \left(\frac{1-Pr}{Pr} \right) \mu^e (u_j u_j)_{,k} \right]_{,k} d\tau$$

$$= - \frac{M_\infty^2}{Re} \int_{R_m} \{\phi\}_{,k} \left(\frac{1-Pr}{Pr} \right)^* \mu^{e*} u_j^* u_{j,k}^* \, d\tau$$

$$= - \frac{M_\infty^2}{Re} \{XMU\}_m^T \{PR\}_m^T [B300OS] \sum_{j=1}^{3} \{U_j\}_m [B211S] \{U_j\}_m \tag{36}$$

In Eq. (36), the repeated subscript j is summed over all scalar components of the velocity vector u_j. The matrix elements of $\{XMU\}_m$ and $\{PR\}_m$ are respectively the m^{th} element nodal values of effective viscosity and the Prandtl Number function. The same operations repeated for the second contribution to dissipation, Eq. (7), yield

$$\int_{R_m}\{\phi\}\left[\frac{1}{Re}\left(\frac{Sc\text{-}Pr}{ScPr}\right)\mu^e\sum_\alpha h^\alpha Y^\alpha_{,k}\right]_{,k}d\tau$$

$$= -\frac{1}{Re}\int_{R_m}\{\phi\}_{,k}\left(\frac{Sc\text{-}Pr}{ScPr}\right)^*\mu^{e*}\sum_\alpha h^{\alpha*}Y^{\alpha*}_{,k}d\tau$$

$$= -\frac{1}{Re}\{XMU\}_m^T\{SC\}_m^T[B300OS]\sum_\alpha\{HS^\alpha\}_m[B211S]\{Y^\alpha\}_m \qquad (37)$$

In Eq. (37), the matrix elements of $\{SC\}_m$ and $\{HS^\alpha\}_m$ are m^{th} element nodal values of the Schmidt Number function and the species static enthalpy, Eq. (10), respectively.

The boundary condition constraint matrices, Eq. (22), are evaluated directly, since they are always applied on the line, x_j equal to a constant. Using prefix A to signify a one-dimensional element operation, obtain

$$\kappa\int_{\partial R_m\cap\partial R}\{\phi\}a^1_m q^*_m d\sigma = \kappa a^{(1)}_m[A200S]\{Q\}_m \qquad (38)$$

$$\kappa\int_{\partial R_m\cap\partial R}\{\phi\}a^3_m d\sigma = \kappa a^{(3)}_m\{A10\} \qquad (39)$$

The A matrices are also listed in Table 5. Equations (33), (35), and (37)-(39) are not presently coded into 3DBR COMOC, but are included here for future reference.

Ordinary Differential Equation System Integration Algorithm

Application of the finite element algorithm to the original partial differential equation has produced a large-order system of ordinary differential equations written on the discretized equivalent of the dependent variable. Several explicit numerical integration algorithms have been developed for ordinary differential equations that are optimum on the multiple bases of stability, accuracy, and required computing time, [Ref. 9, 10].

However, the explicit numerical solution of stable systems of differential equations with large Lipschitz constants creates serious integration step-size restrictions. The integration package in COMOC contains two methods which belong to a family of optimally stable, 3-stage, one-step integration methods [Ref. 11]. The operational features of this integration package, aside from the ease of programming using an explicit procedure, include being one-step (and therefore self-starting), having internal error control features, automatic step-size determination, derivative evaluations required at the integration-interval end points only, and optimal stability and accuracy within their given structure.

The family of numerical integration methods that are one-step, predictor-multiple-corrector formulas, are described by the equations

$$
\begin{aligned}
p_{n+1}^{1} &= a_1^1 q_n + h b_1^1 q_n' \\
p_{n+1}^{2} &= a_1^2 q_n + h[b_1^2 p_{n+1}^{1\prime} + b_2^2 q_n'] \\
&\vdots \qquad\qquad \vdots \qquad\qquad \vdots \\
p_{n+1}^{k-1} &= a_1^{k-1} q_n + h[b_1^{k-1} p_{n+1}^{k-2\prime} + b_2^{k-1} q_n'] \\
q_{n+1} &= a_1^k q_n + h[b_1^k p_{n+1}^{k-1\prime} + b_2^k q_n'] \qquad (40)
\end{aligned}
$$

Two members belonging to the 3-stage family are operational in COMOC. Both methods are first-order accurate, i.e., their associated truncation error is of order h^2, where h is integration step-size, and they represent optimally stable methods within the collection of first-order accurate methods. The coefficients in Eq. (40) for these two methods are listed in Table 6. Method 1 enjoys a large absolute stability interval, while method 2 has an extended relative stability interval. Both options in the integration package attempt to extremize integration step size automatically, based upon internal error control. The estimation of relative truncation error for both methods is of the form

$$
|\mathrm{RTE}| = \frac{h}{\beta}\left[\frac{|p_{n+1}^{2\prime} - q_n|}{|q_{n+1}|}\right] \qquad (41)
$$

where the parameter, β, equals 3 and 6, respectively, for method 1 and 2. Equation (41) is utilized within the integration package to evaluate the relative truncation error associated with using the given integration step size, h, to estimate the $(n+1)^{st}$ value of the dependent variable. If the computed error is less than the user-supplied acceptable limit, the $(n+1)^{st}$ estimate

TABLE 6

COEFFICIENTS IN INTEGRATION ALGORITHM
FOR TWO, ONE-STEP, THREE-STAGE METHODS

Coefficient	Method 1	Method 2
a_1^1	1.000000	1.000000
a_1^2	1.000000	1.000000
a_1^3	1.000000	1.000000
b_1^1	1.000000	1.000000
b_1^2	0.037037	0.074074
b_2^2	0.962963	0.925926
b_1^3	0.148148	0.296296
b_2^3	0.851852	0.703704

for the dependent variable is accepted. Dependent upon computed solution behavior, the integration algorithm will selectively seek to increase h, by some fraction, before proceeding to the next integration computation. In this fashion, the package consistently seeks to increase step size (hence decrease solution computation time). If at any point the computed relative error exceeds the limit, the current predicted values for the dependent variable are discarded, a smaller step size selected, and the operations of Eq. (40) repeated until an acceptable error is measured.

Continuity Equation Solver

Since an explicit integration algorithm is utilized for solution of Eq. (22), solution of Eq. (24) for transverse mass flux ρu_2 is required only after all other dependent variable distributions have been obtained on the plane x_1 = constant. Establishment of $(\rho u_3^*)_{,3}$ is direct since the nodal distribution of $\{\rho U3\}$ is known. However, an evaluation of $(\rho u_1^*)_{,1}$ is required, since no streamwise derivatives of a dependent variable can be formed before the distribution of all variables is known in a plane. In the discretized solution, the actual requirement

is to establish $\{\rho U1\}'$; the following second-order accurate finite difference formula for the derivative at the end point of two panels of data of dissimilar length is employed.

$$\{\rho U1\}'_{n+1} = \frac{1}{h_n h_{n+1}(h_n + h_{n+1})}\left[h_n(2h_{n+1} + h_n)\{\rho U1\}_{n+1} - (h_n + h_{n+1})^2\{\rho U1\}_n + h_{n+1}^2\{\rho U1\}_{n-1}\right] \quad (42)$$

In Eq. (42), h_{n+1} and h_n are the x_1 integration step-sizes, respectively, between the current x_1 station, x_{n+1}, and the previous two stations.

An analytic expression is then established for the x_2 distributions of mass flux derivatives, with x_3 as a parameter and on a nodal basis, as

$$(\rho U1)' = \sum_{k=0}^{n} a_k(x_3)x_2^k$$

$$(\rho U3)_{,3} = \sum_{k=0}^{n} b_k(x_3)x_2^k \quad (43)$$

using an n^{th} order running-smoothing polynomial generator over appropriate sequential panels of data. Using a unit step for the weighting function, Φ, Eq. (24) then takes the form

$$\int_{R_m}\left[(\rho u_2^*)_{,2} - \sum_{k=0}^{n}[a_k(x_3) + b_k(x_3)]x_2^k\right]dx_2 = 0 \quad (44)$$

Since all terms in Eq. (44) are integrals of perfect differentials, the solution for the increment in transverse mass flux over an interval Δx_2 is directly obtained as

$$\Delta(\rho u_2^*) = \sum_{k=0}^{n}[a_k(x_3) + b_k(x_3)]\frac{x_2^{k+1}}{k+1} \quad (45)$$

Repeating Eq. (45) along each node column completes determination of ρu_2^* at the nodes of the transverse plane.

Computation of Equilibrium Composition and Thermodynamic Properties of Hydrogen/Oxygen/Air Mixtures

The 3DBR Variant of COMOC can compute three-dimensional frozen flow mixing of arbitrary gas mixtures, as well as the

equilibrium combustion of hydrogen/oxygen/air systems. For the latter, the NASA computer code GAS (see Ref. 12) has been made operational within COMOC after considerable modification to render it compatible with a marching-type solution with multiple nodes, hence solutions. The equilibrium composition and thermodynamic properties of hydrogen/oxygen/air mixtures are evaluated as a function of temperature and pressure; relative concentrations of the elements, H_2, O_2, N_2, and Ar are also determined. The species considered are H_2O, O_2, H_2, N_2, Ar, O, H, NO, and OH. Since all thermophysical properties are temperature dependent, stagnation enthalpy is typically not known a priori; consequently, initialization is based upon a user input total temperature distribution. As a function of input pressure at initialization and the built-in tables of thermodynamic data, distributions of static temperature, frozen specific heat, and stagnation enthalpy corresponding to input total temperature are determined using an iteration algorithm based upon the method of false position. All solutions following initialization are based upon iteration to equilibrium composition using computed nodal static temperature as the convergence parameter. The iteration on temperature is assumed to have converged when the difference between successive iterates is less than 0.1 percent.

After convergence to a static temperature, the equilibrium constants for chemical reaction are calculated from the Gibbs' function. Composition is then determined using a modified Newton-Raphson iterative procedure for solution of a system of nonlinear algebraic equations. Once the nodal species equilibrium (or frozen) composition is determined, enthalpy, entropy, molecular weight, and specific heat are calculated for mixtures of ideal gases in terms of the computed species mole fractions, X^α, as

Molecular Weight:
$$W = \sum_\alpha X^\alpha W^\alpha \tag{46}$$

Specific Heat:
$$c_p = \frac{1}{W} \sum_\alpha X^\alpha c_p^\alpha \tag{47}$$

Static Enthalpy:
$$h = \frac{1}{W} \sum_\alpha X^\alpha h^\alpha \tag{48}$$

Entropy:
$$S = \frac{R}{W} \sum_\alpha X^\alpha \left[\frac{S^\alpha}{R} - \ln p - \ln X^\alpha \right] \tag{49}$$

Mass Fraction:
$$Y^\alpha = X^\alpha W^\alpha / W \tag{50}$$

Gas Constant:
$$\gamma = \frac{c_p}{c_p - R/W} \tag{51}$$

The equilibrium model is based upon the conservation properties of the sum of mole fractions, and the constancy of the atomic number density ratios of argon/nitrogen, nitrogen/oxygen, and hydrogen/oxygen. The five chemical reactions considered are

$$
\begin{aligned}
2H + O &\rightleftarrows H_2O \\
2H &\rightleftarrows H_2 \\
2O &\rightleftarrows O_2 \\
H + O &\rightleftarrows OH \\
N_2 + 2O &\rightleftarrows 2NO
\end{aligned}
\tag{52}
$$

Applying the Law of Mass Action [Ref. 7] to each reaction in Eq. (52), the following system of nonlinear algebraic equations relating species mole fractions, $X^{(\alpha)}$, is obtained.

$$
\begin{aligned}
X^{(4)} &= K_1 p^2 \left[X^{(1)}\right]^2 X^{(5)} \\
X^{(3)} &= K_2 p \left[X^{(1)}\right]^2 \\
X^{(6)} &= K_3 p \left[X^{(5)}\right]^2 \\
X^{(2)} &= K_4 p X^{(5)} X^{(1)} \\
X^{(7)} &= K_5 p^{1/2} \left[X^{(8)}\right]^{1/2} \left[X^{(6)}\right]
\end{aligned}
\tag{53}
$$

In Eq. (53), K_i is the equilibrium constant for the i^{th} reaction, which is a function of temperature only, and p is the static pressure. The numbering scheme for species identification is listed in Table 7.

TABLE 7

SPECIES IDENTIFICATION FOR REACTING HYDROGEN/OXYGEN/AIR SYSTEMS

Number	1	2	3	4	5	6	7	8	9
Chemical Species	H	OH	H_2	H_2O	O	O_2	NO	N_2	Ar

Equations for the conservation of total mass, and the individual atomic species H, O, N, and Ar, may be expressed in terms of known constants by the matrix equation.

$$[N_{\alpha}^{\beta}]\{X^{\alpha}\} = \{\text{const.}\} \tag{54}$$

where

$$[N_{\alpha}^{\beta}] \equiv \begin{bmatrix} 1 & 1 & 1 & 1 & 1 & 1 & 1 & 1 & 1 \\ 1 & 1 & 2 & 2 & 0 & 0 & 0 & 0 & 0 \\ 0 & 1 & 0 & 1 & 1 & 2 & 1 & 0 & 0 \\ 0 & 0 & 0 & 0 & 0 & 0 & 1 & 2 & 0 \\ 0 & 0 & 0 & 0 & 0 & 0 & 0 & 0 & 1 \end{bmatrix} \tag{55}$$

and

$$\{\text{const.}\} \equiv \begin{Bmatrix} 1.0 \\ c^{(1)} \\ c^{(2)} \\ c^{(3)} \\ c^{(4)} \end{Bmatrix} \tag{56}$$

The specific values of the constants $c^{(\beta)}$ are determined from the initial composition.

Of the several possible choices, the computed composition is based upon solution of the nonlinear equilibrium equations for mole fraction of hydrogen, atomic oxygen, and the square root of molecular nitrogen. The resultant nonlinear equation system requiring solution is

$$[f_i(X^{\alpha})]\{X^{\alpha}\} = \{0\} \tag{57}$$

The Newton-Raphson iteration algorithm assumes, given a set of trial values, X_n^{α}, determination of a new set of values X_{n+1}^{α}, separated from the initial estimate by ΔX_n^{α}, by differentiating Eq. (57) to yield.

$$[J(f_i, X^{\alpha})]\{\Delta X_n^{\alpha}\} = -\{f_i(X_n^{\alpha})\} \tag{58}$$

In Eq. (58), the Jacobian contains elements, $j_{k\ell}$, determined numerically as

$$j_{k\ell} \equiv \frac{\partial f_k}{\partial X_{\ell}^{\alpha}} \tag{59}$$

The $n+1^{st}$ estimate of X^{α} is accepted as the solution to Eq. (58) when

$$\sum_{j=1}^{3} |f_j(X^{\alpha}_{n+1})| \leq \varepsilon \qquad (60)$$

where ε is a prescribed small parameter, usually 10^{-5}. A maximum of thirty iterations are allowed for the solution of Eq. (57)-(60) to converge within ε. In only a few cases has non-convergence occurred, always within a few degrees of the threshold temperature for dissociation. For these initially divergent solutions, the equations are resolved assuming that dissociation is negligible, i.e., the mole fractions of H, O, OH, and NO are negligibly small in comparison to H_2, O_2, N_2, and H_2O.

ILLUSTRATIVE SOLUTIONS

The 3DBR Variant of COMOC has established solutions for several two- and three-dimensional boundary region flows covering a wide range of Mach and Reynolds numbers. Several are discussed to illustrate the various features of solution. The data decks for two of these cases are presented in the next section, and come as standard test cases with the program.

Constant Density Flow Fields

Because of its basic simplicity, the two-dimensional, isoenergetic, laminar boundary layer flow of a fluid at small Mach number ($M < 0.3$) provides an excellent check case for evaluating the essential performance features of the finite element algorithm for Eq. (15)-(17). Only one dependent variable (u_1) need be integrated numerically, along with solution of the continuity equation for u_2. However, COMOC assumes all flows are three-dimensional and compressible with temperature-dependent thermophysical properties. The two-dimensionality is readily obtained by specifying only one column of elements, see Fig. 4, and enforcing the vanishing normal gradient ($q_{,n} \equiv 0$) boundary condition on the lateral segments of ∂R. This is particularly simple since vanishing gradient is the automatic default value intrinsic to the finite element algorithm. The discretization may be extended beyond the boundary layer thickness, δ_x, so that vanishing normal gradient may be applied along the freestream segment of ∂R as well. The slope of the diagonals of the discretization, Fig. 4, bears little impact on solution accuracy for two-dimensional problems. Dependent upon initial conditions and/or other perturbations placed into the solution, the computed variable distributions along each node column may differ slightly. These

small differences typically damp out as the solution proceeds, and interchanging diagonal slopes simply exchanges the location of these differences if they exist. The element aspect ratio is similarly unimportant for two-dimensional problems. For isoenergetic flows, COMOC contains a simple but quick-running subroutine to compute density and static temperature for two-component perfect gas mixtures with a specified pressure distribution. Unless overridden by a user-supplied subroutine, viscosity is computed from Sutherland's law.

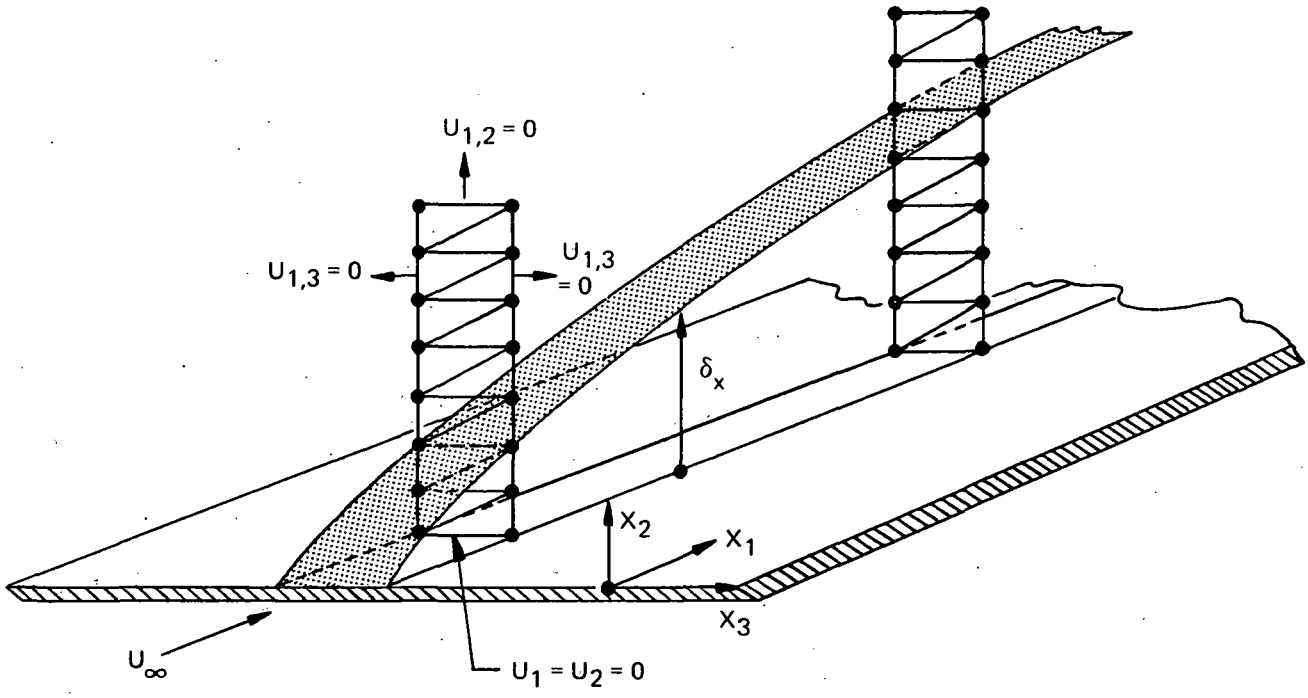

Figure 4. Finite Element Discretization for Two-Dimensional Boundary Layer Flow

Assessment of computed solution accuracy and convergence with discretization can be obtained for the vanishing pressure gradient case by comparison to the Blasius similarity solution [Ref. 13]. The test case corresponds to air at atmospheric pressure and M = 0.272. The boundary layer thickness at the initial station is δ_0 = 0.0011 m. ($\equiv$ 0.11(-2)) and the unit Reynolds number is Re_x = 0.63(7)/m. Two uniform discretizations were employed, the first spanning δ_0 with only four (4) finite elements, while the second doubled that number. The numerical computations were initialized with the similar solution profiles at a station downstream from the leading edge at x_1/δ_0 = 278. The solution was continued downstream to x_1/δ_0 = 2560. Shown in Fig. 5 is a comparison of the Blasius solution to the computed velocity profiles, u_1 and u_2, obtained for the coarser discretization. For reference purposes, the initial profiles

are also shown with the finite element node locations superimposed. The longitudinal flow initially contained within δ_0 has been retarded by a factor of 2 to 3 throughout, and agreement between the computed and Blasius velocity profiles is excellent. The computed skin friction and displacement thickness distributions are shown in Fig. 6. The computations using the coarser discretization slightly underpredict skin friction and over estimate displacement thickness. Doubling the discretization (to 8 elements lying within δ_0) noticeably improves computed solution agreement with the Blasius solutions, Fig. 6. Figure 7 presents actual percent inaccuracy in the computed solutions for skin friction and displacement thickness. The influence of the coarse discretization is most noticeable in δ; however, the error rapidly decreases as the boundary layer grows into the discretization, which corresponds essentially to grid refinement. As a function of discretization, computed skin friction, C_f, converges approximately proportional to the square of refinement. This agrees exactly with the convergence rate predicted theoretically for the parent diffusion equation, neglecting convection, using linear finite element approximation functionals [Ref. 14]. The uniformly small inaccuracies in computed skin friction for both discretizations indicate that solutions, adequate for certain engineering approximations, can be obtained using finite element discretizations that appear rather coarse in comparison to conventional experience.

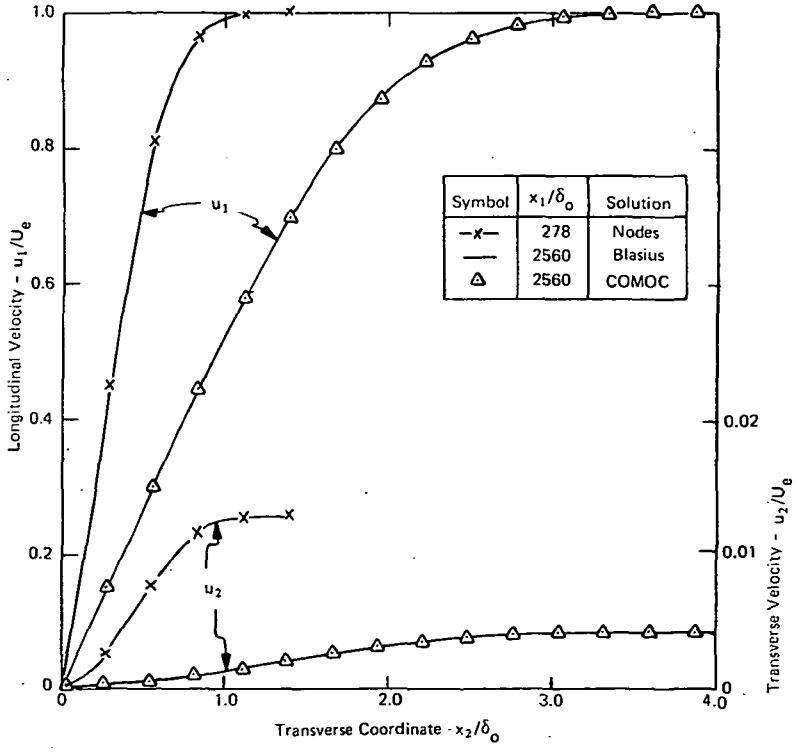

Figure 5. Computed Velocity Distributions, M = 0.272, Re_x = 0.63(7)/m

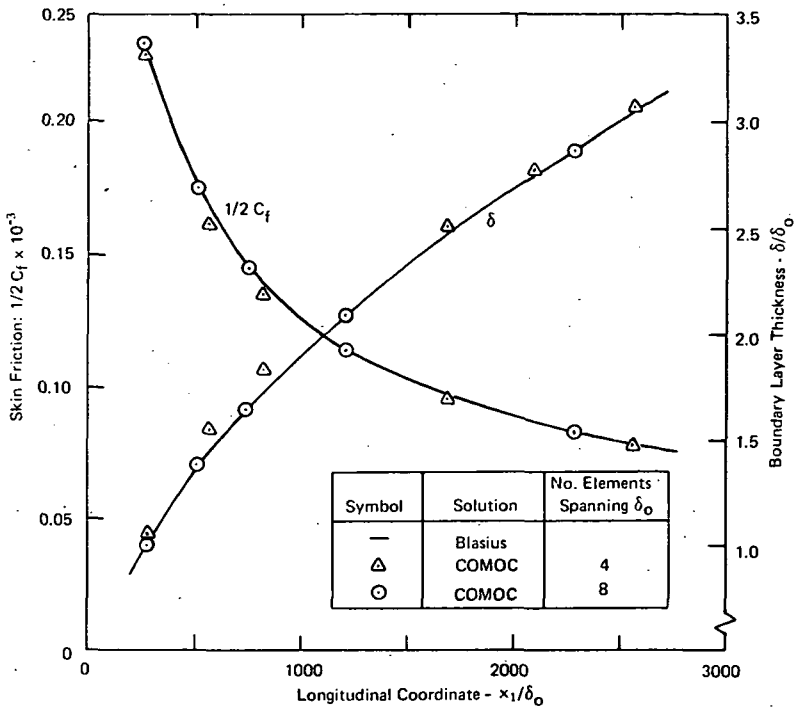

Figure 6. Computed Skin Friction and Boundary Layer Thickness, M = 0.272, Re_x = 0.63(7)/m

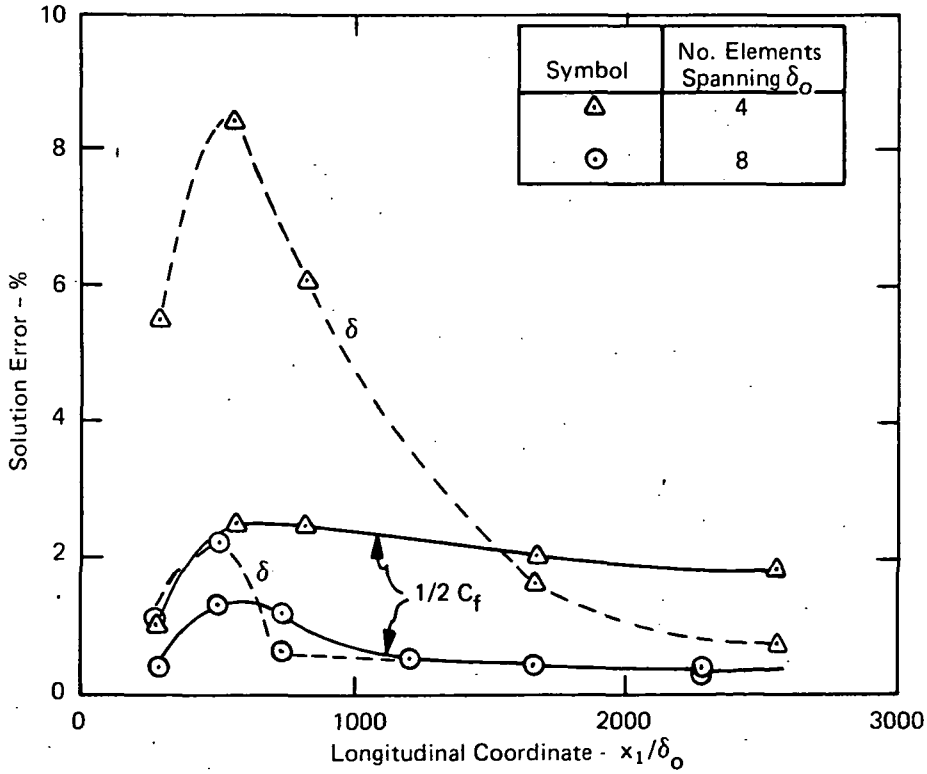

Figure 7. Computed Solution Accuracy and Convergence, M = 0.272, Re_x = 0.63(7)/m

The increased accuracy of the finer discretization solutions is obtained with a measurable increase in computer CPU time. Shown in Fig. 8 are the distributions of integration step-size, $\Delta X1$, automatically established by COMOC as within the stability interval of the Method 1 integration algorithm for this boundary layer problem. The periodic stepping feature is illustrated for the four element solution; the step-size of the eight element solution remains essentially constant at about one-fourth the average of the former. Since the finer discretization contains twice as many elements as well, an approximate eight-fold increase in computer time would be anticipated. The actual increase was by a factor of 6.9, see Fig. 8. Computer CPU is also a function of the number of dependent variables in the solution, as well as user utilization of the I/O features of COMOC. An approximate formula for estimating execution time in seconds is

$$CPU = \lambda \sum_i c_i \qquad (61)$$

where λ is the ratio of CP speed of the computer in use to that of the IBM 360/65 (e.g., $\lambda \approx 0.2$ for the CDC 6600), and

$$c_1 \equiv 0.011 \times (\text{No. elements}) \times (\text{No. passes}) \times (\text{No. dependent variables} + 0.165)$$

$$c_2 \equiv 0.8 \times (\text{No. outputs}) \times (\text{No. pages per output})$$

$$c_3 \equiv 1.25 \times (\text{No. outputs if Restart tape is written})$$

In the expression for c_1, the number of passes is an output parameter from COMOC that is somewhat greater than three times the number of integration steps in the solution. The factor 0.165 accounts for simple thermodynamic, viscosity, and other parameter evaluations. The contribution from c_3 occurs only when writing a restart tape, and the coefficient may vary with different computers.

A second illustrative solution for 3DBR COMOC in the low speed category comes from environmental hydrodynamics. Analytical prediction of thermal and/or waste water dispersion into waterways could help understand the important mechanisms for turbulent transport phenomena. Such a capability could also circumvent some of the detailed laboratory experimentation now required for certification of engineering projects. The example [Ref. 15] corresponds to turbulent dispersion of ejectant from a submerged waste water outfall. The solution domain is non-regular and corresponds to the measured cross-sectional depth distribution of a natural stream [Ref. 16] with a span of 48 m. (160 ft), see Fig. 9. The initial longitudinal velocity distribution was established from the measured isovel distribution,

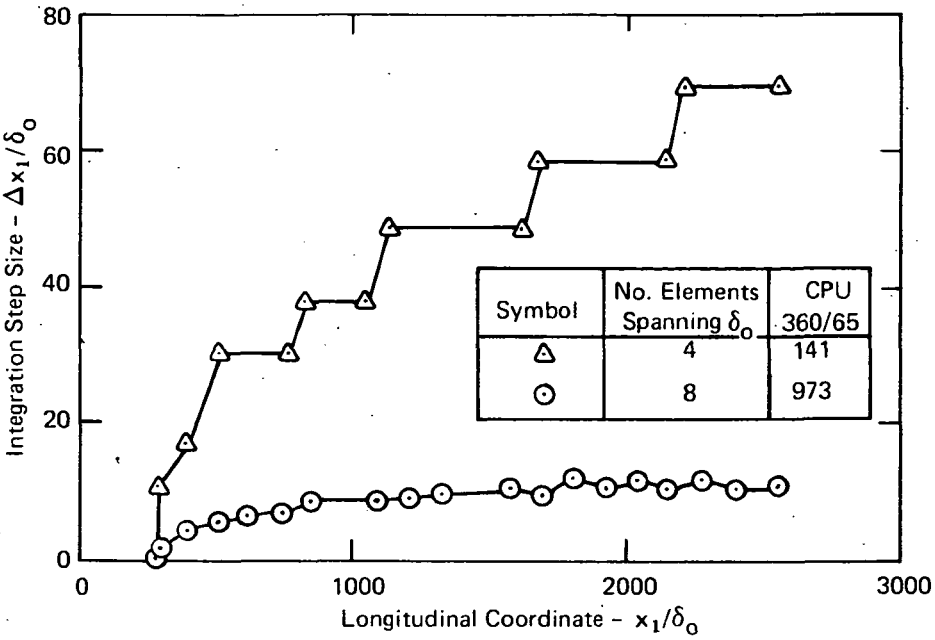

Figure 8. Integration Step-Size Distribution, $M = 0.272$, $Re_x = 0.63(7)/m$

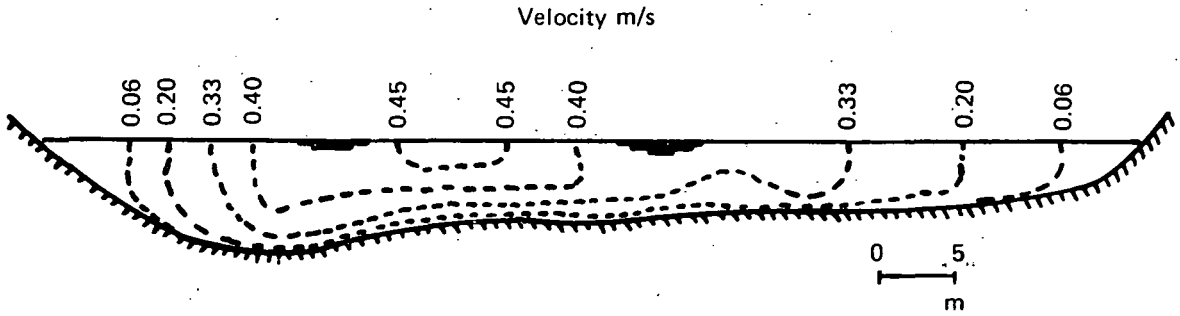

Figure 9. Cross-Section of a Natural Stream Showing Measured Isovels, [Ref. 16]

by interpolation at the nodes of a 468 finite element discretization of the cross-section, see Fig. 10. Since the solution domain is quite non-regular, the automatic discretizer in COMOC was not applicable. The waste water ejector was assumed located in the deepest section of the river as shown in Fig. 10.

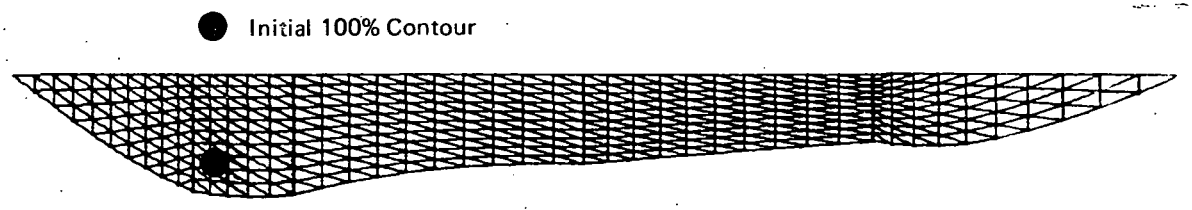

Figure 10. Finite Element Discretization of Stream Cross-Section

The flow field was assumed isoenergetic and without cross-flow. Hence, a marching type solution was required for mainstream velocity and a single species mass fraction. The total and static temperatures for this case are identical; thus, a large input pressure was employed to coerce the perfect gas subroutine in COMOC to compute a uniform density distribution corresponding to that of water. Closure of the governing equation system was obtained by specifying a turbulent viscosity law, and providing a user-written subroutine to override Sutherland's Law. A tensor turbulence law was assumed applicable [Ref. 17, 18]; in the plane of the finite element discretization, the eddy viscosity coefficients in the vertical (x_2) and transverse (x_3) coordinate directions were assumed given as

$$\mu^e_{12} = k_2 U^* h \tag{62}$$

$$\mu^e_{13} = k_3 U^* h \tag{63}$$

where local depth of water is given by h, k_2, and k_3 are empirical constants, and U^* is the friction velocity defined as $U^* \equiv \sqrt{\tau}/\rho$. The approach of Patankar and Spalding [Ref. 19] was employed to evaluate wall shear, τ, as.

$$\tau \equiv K^2 \rho \tilde{U}^2 [R_x^{-1} - 0.156 R_x^{-0.45} + 0.08723 R_x^{-0.3} + 0.03713 R_x^{-0.18}] \tag{64}$$

where K is an empirical constant (set equal to 0.435), $R_x \equiv R K^2$ where R is a local Reynolds Number defined as $R \equiv \rho \tilde{U} \tilde{x}_2 / \mu$, $\tilde{U}$ is local longitudinal velocity near its extremum, and $\tilde{x}_2$ is a representative length scale. For the present case, both $\tilde{U}$ and $\tilde{x}_2$ were obtained directly from the solution for the detailed velocity profiles. A study was performed, see Table 8, to measure the sensitivity of the computed pollutant distribution to the constants in the eddy viscosity law, Eq. (62)-(63), as well as the tensor character. The base line case corresponds to use of mean depth averages for the coefficients, confirmed experimentally to capture the essential parabolic character of the measured distributions, Case II. Case III corresponds to a scalar eddy viscosity equal to the magnitude of the Case I tensor expression.

The results obtained from this type of study are summarized in Fig. 11, which presents predicted mass fraction contours of the contaminant, for the three cases, at a station 9.6 m. downstream of injection. Comparing the results of Cases I and II, the neglect of the parabolic distribution in the vertical mixing

TABLE 8

PARAMETERS IN POLLUTANT DISPERSION STUDY

Case	k_2	k_3	Comments
I	0.067	0.23	Base line case [Ref. 16]
II	$0.36(\xi-\xi^2)$	0.23	Vertical parabolic distribution (ξ=nondimensional local depth)
III	0.24	0.24	Scalar of equal magnitude to Case I

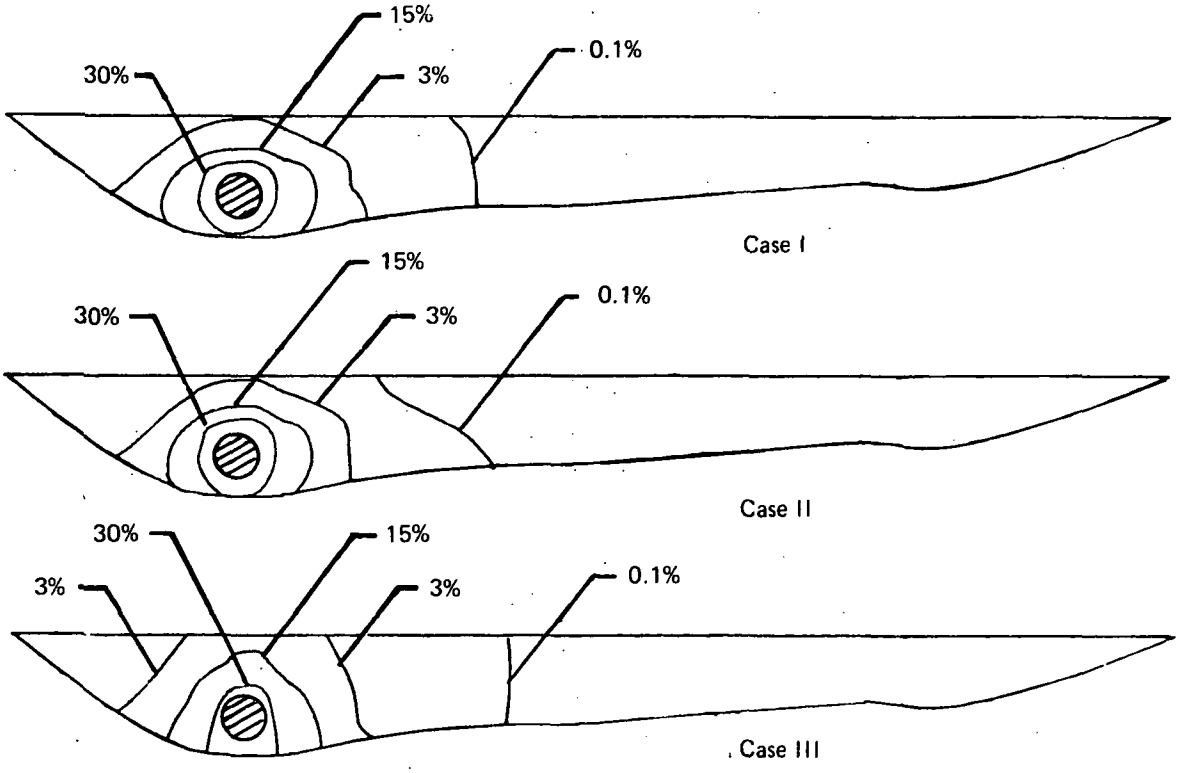

Figure 11. Predicted Mass Fraction Contours at 9.6 m Downstream of Injection, Three Diffusion Models

coefficients is confirmed to be a reasonable assumption at this distance downstream. However, for these conditions, the omission of the tensorial character of the dispersion coefficient, Case III, is quite measurable. Comparing Cases III and II, the larger vertical (k_2) coefficient has allowed the 3% contour to break to the surface of the river. An overall larger diffusion has also

occurred, although, as expected, the lateral extent of the distributions is considerably less affected. Although no experimental data are available to directly confirm these results, these predictions amply illustrate the potential to examine trends and isolate key features, while capturing the important geometric non-regularities and differential equation non-linearities so important to the physics of the problem. The numerical procedure is readily adaptable to relocation of the ejector and alteration of its geometry, see Fig. 12 for example. For all cases, integration was continued downstream a distance of approximately 90 m; at this point the maximum ejectant concentration had decreased to

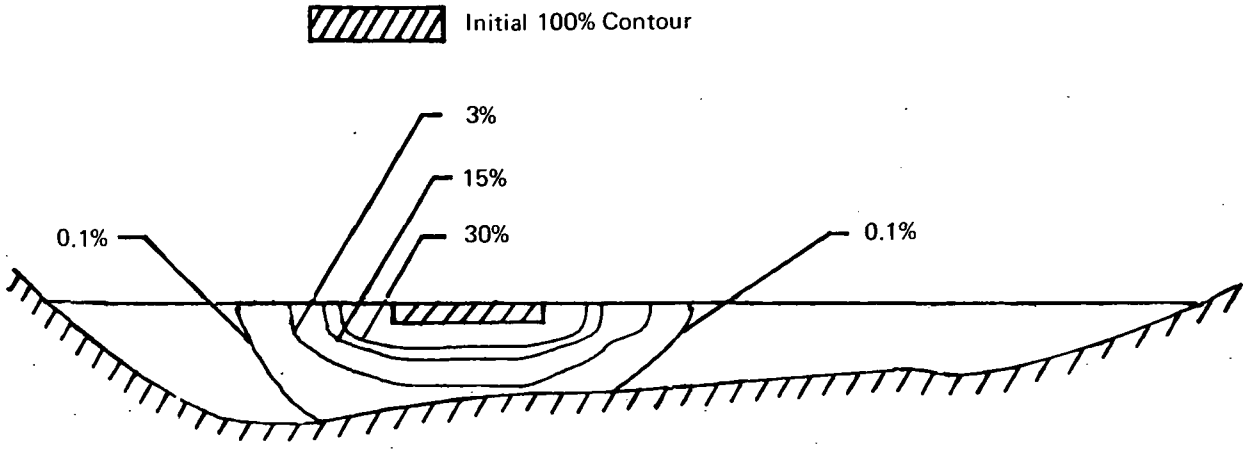

Figure 12. Predicted Mass Fraction Contours at 9.6 m Downstream of Interface Injection

15% ±1% dependent upon the viscosity law. A typical execution time on the IBM 360/65 was 875 s including about 145 s to produce an inch of output. The predicted value using Eq. (61) is 900 s. (It should be noted that, although tensor turbulent transport properties can be utilized in 3DBR, program modification, beyond the scope of the casual user, is required for the present Variant.)

Compressible Flow Fields

A standard check case for 3DBR COMOC corresponds to a nominal Mach 5 laminar, two-dimensional boundary layer flow over an adiabatic wall in a favorable pressure gradient. A similarity solution [Ref. 20], as well as finite difference procedures, can be utilized to evaluate accuracy and consistency of solution trends for the detailed coupling of the mechanics and thermodynamics of this solution. The discretization and boundary condition specifications are essentially identical to those of the small Mach number boundary layer solution. For constant specific heat, which corresponds to the similarity solution, the simple thermodynamic subroutine can be used to compute local static temperature and density for isoenergetic flow. Only the equation for u_1 need be integrated downstream, coupled with solution for u_2 using the

continuity equation solver. For non-isoenergetic flow or variable specific heat, stagnation enthalpy (H) must be added to the integrated solution vector, and the local solutions for density, static temperature, and specific heat are obtained from the combustion subroutine. In this instance, the air composition must be initialized as well, although the oxygen and nitrogen elemental species mass fractions need not be integrated since the flow field composition is homogeneous and constant. For either thermodynamic procedure, the stagnation enthalpy is initialized from an input (constant) total temperature distribution. The initial u_1 profiles are established from the similar solution for $\beta = 0.5$ and $S = 0$ [Ref. 20]. Sutherland's law is employed to compute viscosity.

The standard test case is initialized at $x_1 = 0.03$ m downstream from the surface leading edge. The boundary layer thickness at this station is $\delta_0 = 0.0039$ m, the local Mach number is $M = 3.77$, the unit Reynolds number is $Re_x = .83(5)/m$, and the adiabatic wall temperature is $T_w = 1000°K$ (1800°R). Shown in Fig. 13 are the COMOC computed skin friction, freestream Mach number, and boundary layer thickness distributions for the constant specific heat case. These were obtained using two uniform finite element discretizations corresponding to 4 and 8 elements spanning the initial boundary layer thickness. The input static pressure distribution, $p_e(x_1)$, is also presented for reference, and the boundary layer thickness has increased greather than four-fold within the solution domain. Only small differences, on the order of about 2%, exist between the two solutions, with the finer discretization producing a slightly larger skin friction and smaller freestream Mach number. Superimposed in Fig. 13, for comparison purposes, are the results for the similar solution [Ref. 20], and a 20 zone finite difference solution obtained using the von Mises coordinate transformation [Ref. 19]. Agreement among the four solutions is excellent (within 2%) for skin friction. The similar solution for M_e lies between the COMOC and finite difference solutions, and agreement is within ±3%. Shown in Fig. 14 are computed velocity profiles at $x_1/\delta_0 = 22.7$, which is about mid-way through the standard test solution domain. Shown for reference is the initial u_1 profile obtained from the similar solution [Ref. 20], with the node locations of the 4 element discretization superimposed. Both COMOC solutions produce u_1 distributions that are slightly more concave upward in the mid-region in comparison to the similarity or finite difference solutions. The finer discretization COMOC solution lies closer to the similarity solution in the region where the two finite element solutions differ. The finite difference solution lies appreciably below both the COMOC and similarity solutions near freestream. The COMOC computed transverse velocities are also shown in Fig. 14; only slight differences between the two discretization solutions are apparent. The trends of

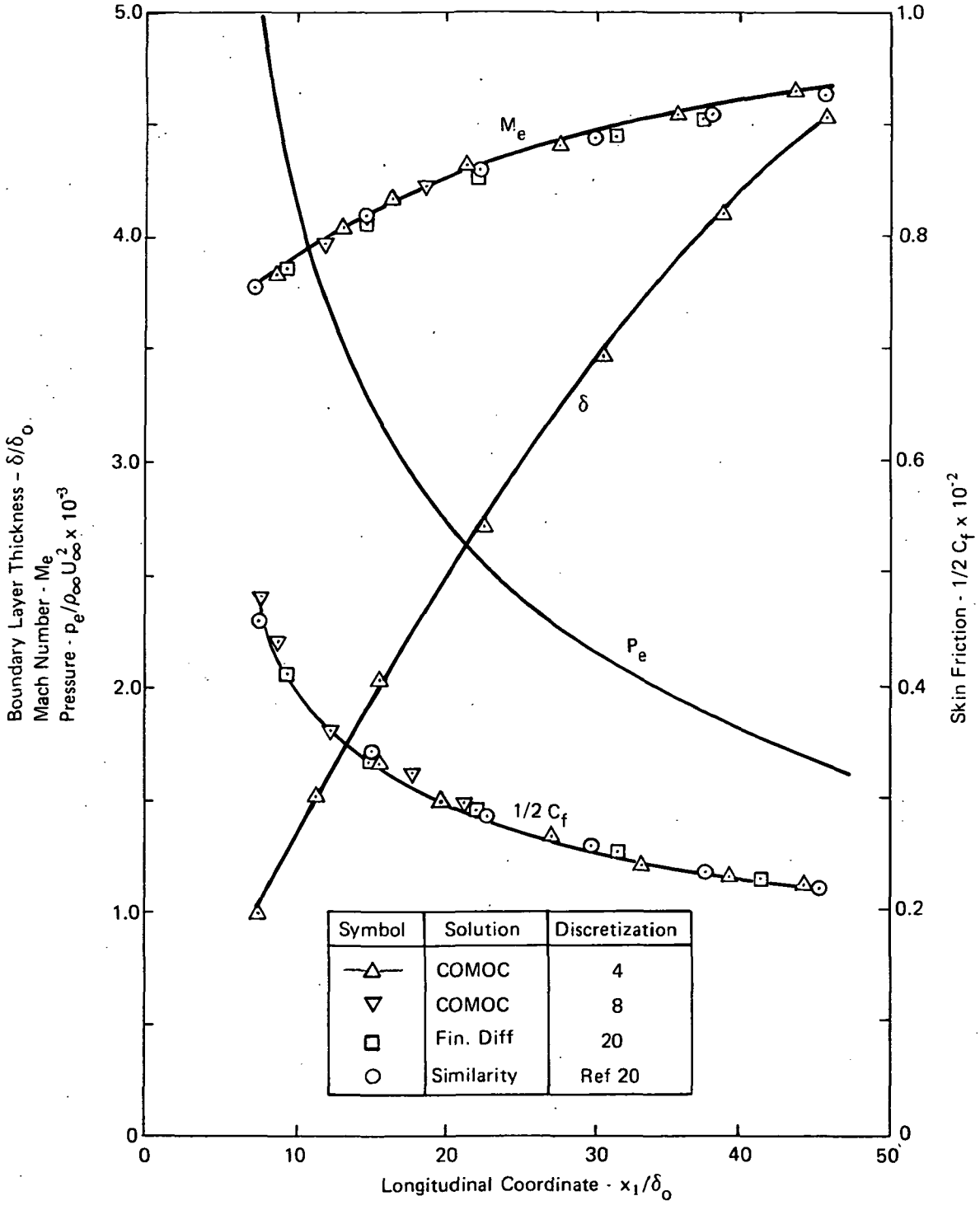

Figure 13. Computed Supersonic Boundary Layer Parameters, $M = 5$, $Re_x = .83(5)/m$, $\beta = 0.5$

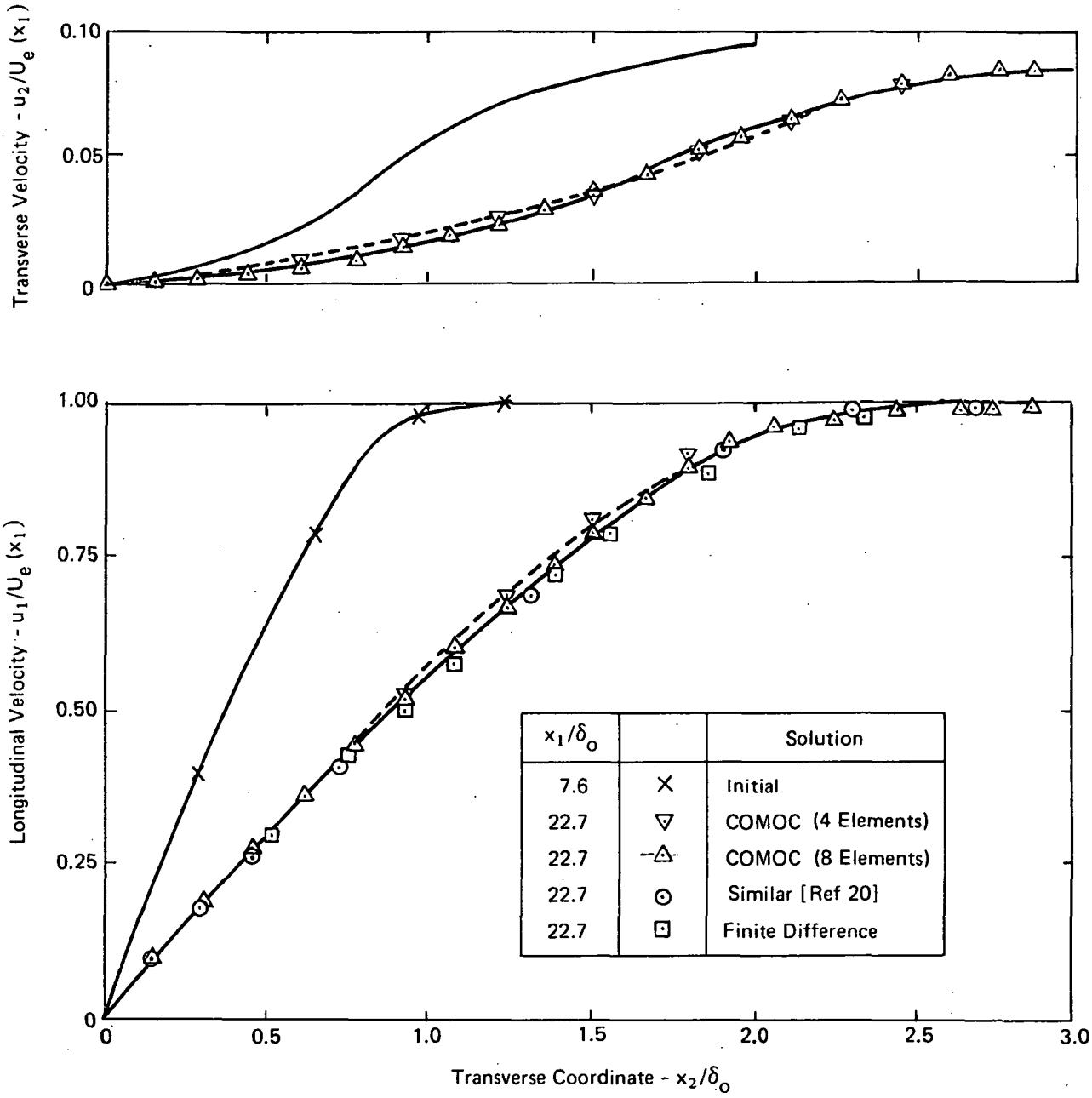

Figure 14. Computed Supersonic Boundary Layer Velocity
$M = 5$, $Re_x = .83(5)/m$, $\beta = 0.5$

the COMOC solutions are in excellent agreement with the established procedures; unfortunately, since each method of solution is distinctly numerical, no absolute accuracy assessment is established, as was possible for the constant density boundary layer check case.

The computation of transverse velocity warrants additional comment. COMOC will accept, but does not require (since one is rarely available), an input distribution for u_2 at the initial station. For the discussed Mach 5 solutions, the initial u_2 distribution, Fig. 14, is self-determined by withholding its computation until the u_1 equation had been integrated forward a few stations. (This is mandatory, even if an initial u_2 distribution is input, since several data stations are required to allow evaluation of Eq. (42) for $(\rho u_1)'$.) Computation of u_2 is then initiated and it rapidly becomes consistent with the computed u_1 distributions. Solution is terminated after a few more steps downstream, and the computed nodal u_2 distribution trend with longitudinal distance is back extrapolated to estimate an initial distribution. Only one or two iterations of this type are typically required to establish a consistent u_2 distribution. Starting with a zero initial distribution is probably the most convenient choice for analysis of engineering problems, wherein detailed initial accuracy is not of primary importance.

Solution speed and accuracy have been illustrated to depend directly upon discretization. Solution speed is also a direct function of a user input control parameter (ε) that places somewhat flexible bounds on acceptable relative truncation error, Eq. (41), during downstream integration. A value of ε of 10(-4) has been found by experimentation to be generally adequate to maintain solution stability, hence accuracy. Using smaller values of ε sharply increases computation time without producing the attendant increase in solution accuracy that a finer discretization would yield. However, increasing ε up to 10(-2) can produce measurable cost savings with a good probability of only a marginal decrease in solution stability and accuracy (upon rare occasion, the solution may actually go unstable and blow-up). Shown in Fig. 15 are computed integration step-size histories for the Mach 5 test case for several discretizations and values of ε. In all cases, the computed solutions were of comparable accuracy and uniformly acceptable. The automatic stepping feature is illustrated, and the predicted necessary sharp decreases in Δx_1 appears independent of ε. For the two, 8-element discretization tests, increasing ε to 10(-2) about doubled the allowed step size and hence decreased CPU by almost 50%. As expected, a four-fold increase in CPU accrued for twice the discretization, for ε constant at 10(-4), with integration step-size about half that of the baseline 8-element case. The coarsest 4-element discretization test recorded the largest integration step distribution with a remarkably smaller CPU. However, this solution appeared on the

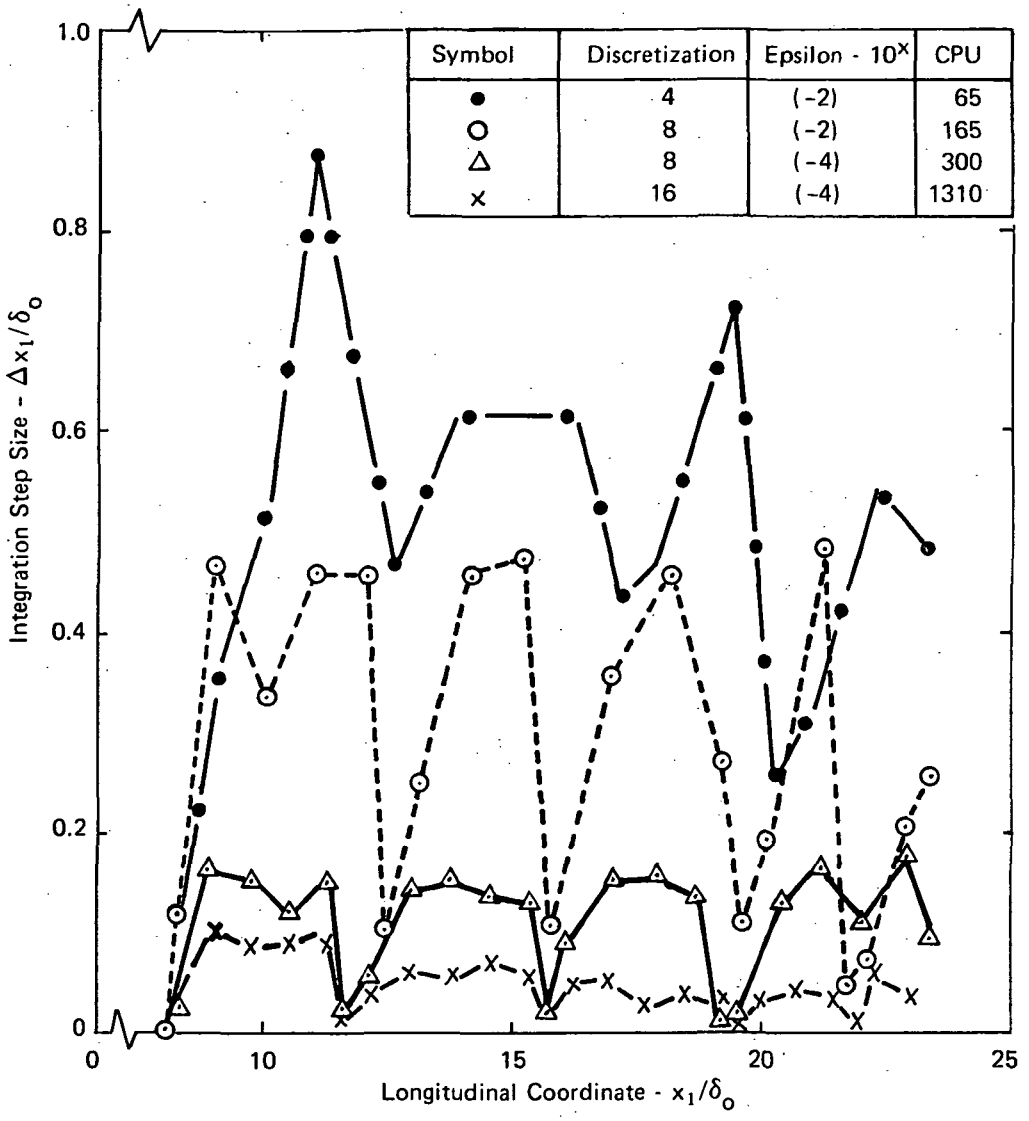

Figure 15. Integration Step Size Distribution, $M = 5$, $Re_x = .83(5)/m$, $\beta = 0.5$

ragged edge of instability, as evidenced primarily by sometimes anomalous behavior in transverse velocity, u_2. From experimentation, incipient overall solution instability is almost always foretold by erratic behavior of the computed u_2 distribution, since it immediately reflects anomalies in the streamwise derivative distribution for u_1, see Eq. (45). The user may typically feel confident that solutions generated using $\varepsilon > 10(-4)$ are acceptable provided the computed u_2 behavior is smoothly consistent. However, it is worthwhile to substantiate this assumption, by a shorter run at smaller ε and/or finer discretization, if it can be afforded

As a final evaluation, the nominal Mach 5 test case was repeated for temperature-dependent specific heat. This necessitates addition of stagnation enthalpy, H, to the dependent variable vector and addressing the thermodynamic package in the combustion subroutine. Shown in Fig. 16 is a comparison between

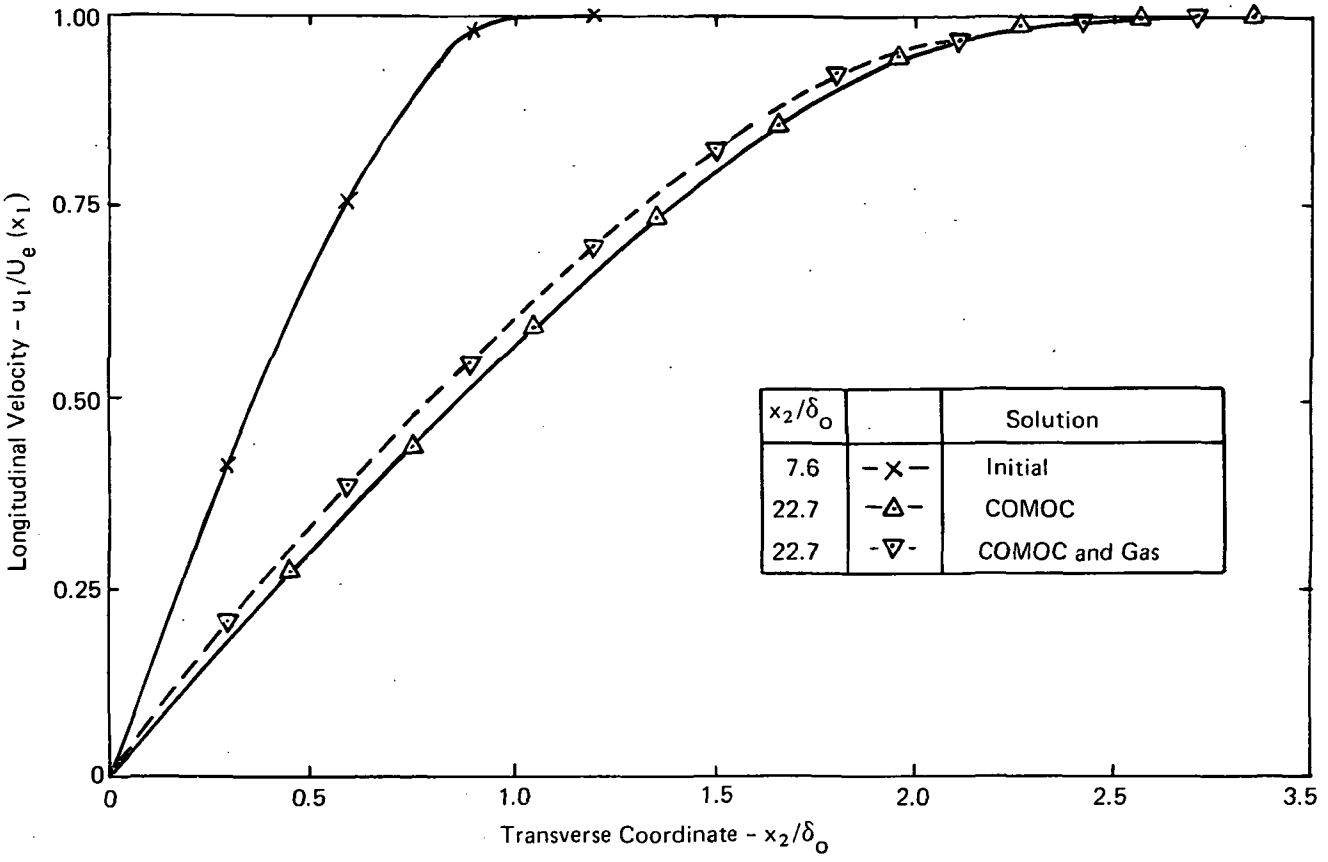

Figure 16. Computed Boundary Layer Velocity Profiles, $M = 5$, $Re_x = .83(5)/m$, $\beta = 0.5$

computed longitudinal velocity distributions at $x_1/\delta_o = 22.7$ for a uniform adiabatic wall temperature of 1000°K. Maximum differences of about 4% accrue due to temperature dependent specific heat; the computed increase in skin friction is about 10%. Besides the increased solution cost stemming from employing H as a dependent variable, an additional expenditure accrues from addressing the more comprehensive thermodynamics package for variable thermophysical properties. Referring to Eq. (61), a fourth contribution to CPU for non-combustion utilization of the combustion subroutine is

$$C_4 \equiv 0.004 \times (\text{No. Passes}) \times (\text{No. Nodes})$$

The second example problem for compressible flow computations using 3DBR COMOC corresponds to analysis of turbulent, binary three-dimensional mixing in a supersonic boundary layer flow field. The analyses include cold flow studies with comparison to data as well as equilibrium combustion. The impetus for these studies is the hydrogen fueled scramjet engine, a prominent candidate for propulsion of the next generation of hypersonic cruise vehicles [Ref. 21, 22]. Many alternative designs have been proposed, but all exhibit the commonality that fuel introduction arrangements consist of rows of circular, choked-flow injector orifices mounted flush or normal to the combustor wall or in fins spanning the combustor inlet. The pattern of fuel injection, hence three-dimensional mixing, can exert significant influence on combustor performance. Figure 17 illustrates an experimental apparatus used by Rogers to experimentally probe the three-dimensional cold mixing region downstream of transverse hydrogen injection from a single discrete orifice [Ref. 23], and multiple laterally-disposed orifices [Ref. 24], into a Mach 4 airstream on a flat plate. Detailed numerical predictions of turbulent, three-dimensional mixing in

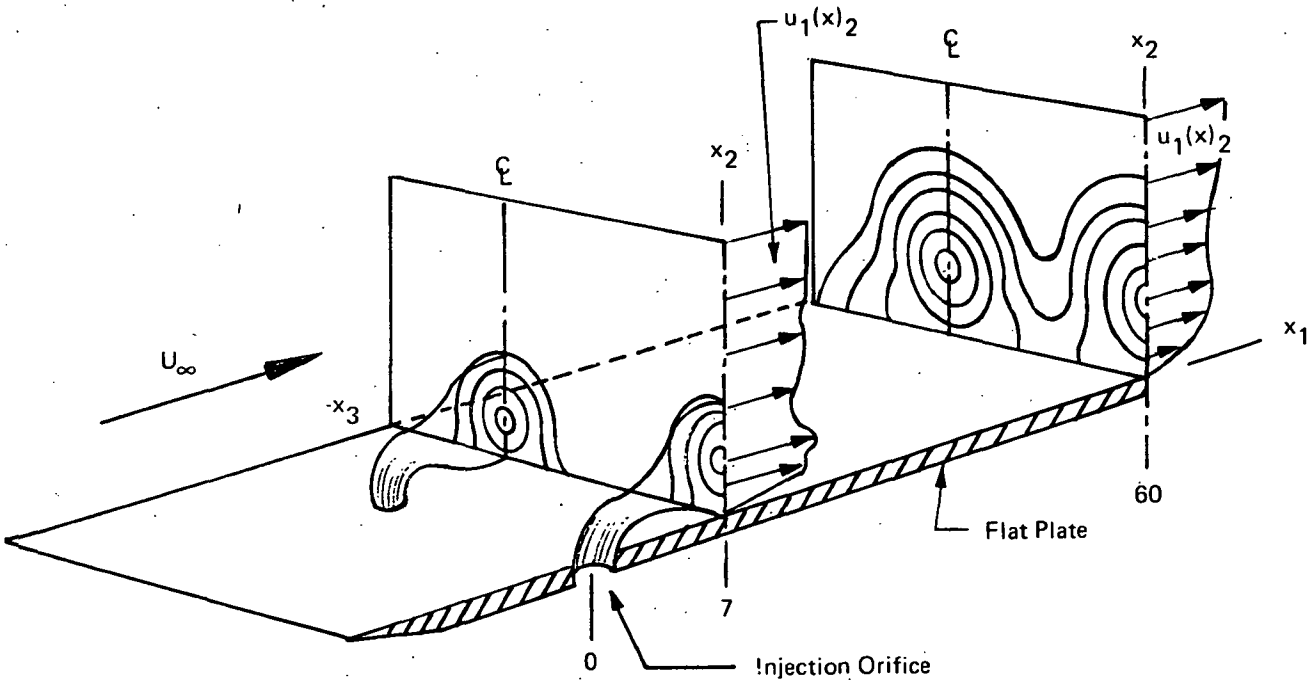

Figure 17. Three-Dimensional Flow Field Downstream of Transverse Injection from Discrete Orifices

this flow field have been performed, using 3DBR COMOC, in a solution domain spanning up to 120 injector diameters downstream, for both the single and multiple jet geometries. The scaled discretization of the symmetric half-plane into 100 finite elements, Fig. 18, was formed by the automatic discretizer. The turbulent boundary layer thickness at the injector station (without injection) was equal to 2.7 injector diameters, and the Reynolds number was $Re_x = .6(8)/m$. To the first order of approximation, these data correspond to isoenergetic binary diffusion in a constant pressure flow field. Hence, numerical integration was required for u_1 and a single species mass fraction plus the continuity equation for u_2.

Closure of the equation system requires a turbulence model for three-dimensional boundary region flow of this type. A prototype eddy viscosity model was developed to reflect mass flux differences between the main flow and the jet and the turbulence due to the presence of the wall [Ref. 25]. Directly above the mixing region, turbulent dispersion was assumed to primarily reflect differences in mass flux. Outside the mixing region but near the wall, the turbulence was assumed due solely to boundary layer phenomena. Within the mixing region both mechanisms are assumed active. Therefore, near the wall where

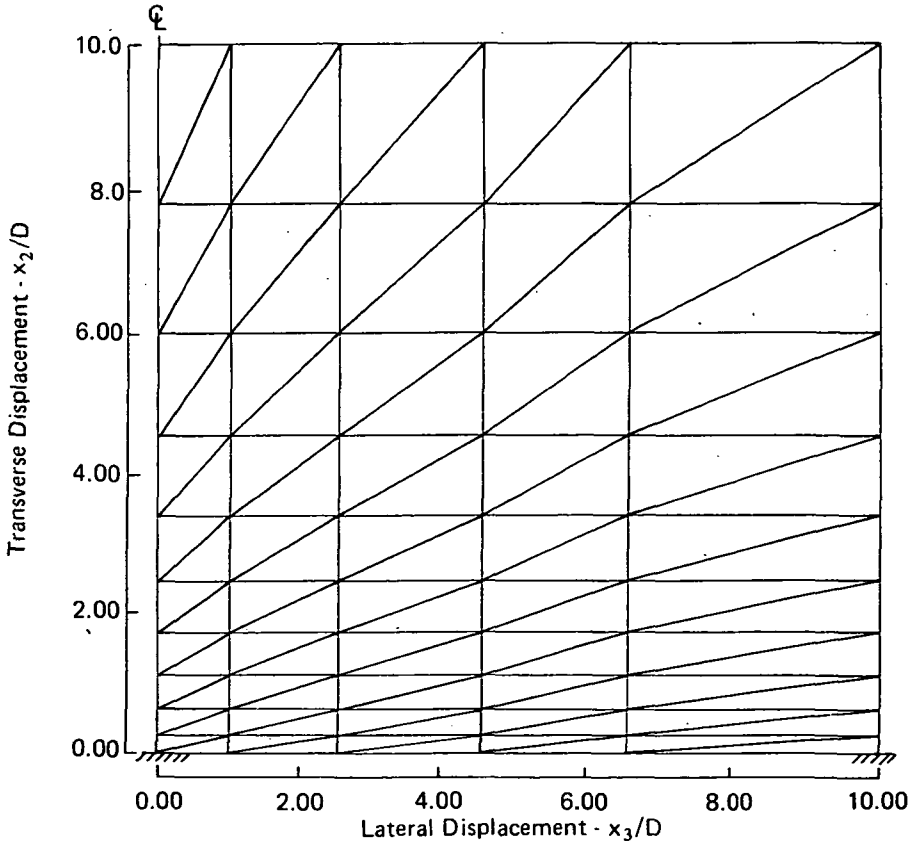

Figure 18. Finite Element Discretion of Symmetric Half-Space of Single-Jet Injection Geometry

mixing length theory is assumed valid, the eddy diffusivity of mass is of the form

$$\varepsilon_1 = \ell^2 \omega \gamma \left| \frac{\partial U_1}{\partial x_2} \right| Sc_T^{-1} \tag{65}$$

u_1 is the mean longitudinal velocity, ℓ is the mixing length, ω is van Driest's damping factor [Ref. 26], and γ is the intermittency factor, empirically modeled in a number of ways [Ref. 27]. For this study, it was evaluated as

$$\gamma = \frac{1}{1 + 0.01\zeta^9} \tag{66}$$

where $\zeta = x_2/\delta_2$, and δ_2 is the value of x_2 where the hydrogen mass fraction is one-half its wall value. In the outer region, the eddy diffusivity of mass is assumed proportional to the mass defect of the form

$$\varepsilon_2 = K\gamma I/\rho L \tag{67}$$

where K is an empirical constant, γ is the intermittency factor, the characteristic length L is defined as the half height of the mixing region on the centerplane ($x_3 = 0$), and I is the three-dimensional mass defect evaluated as

$$I(x_1) \equiv \int_R |\rho u_1 - \rho_\infty U_\infty| d\tau \tag{68}$$

A subroutine was coded for addition to 3DBR-COMOC, to evaluate Eq. (65)-(68) along columns of nodes parallel to the x_2 axis, see Fig. 18. The effective viscosity of mass mixing was laminar plus selectively ε_1 or ε_2, and the transition from ε_1 to ε_2 was internally signaled. So as to provide the potential user with an example of construction of a fairly complex subroutine addition, this code forms a part of the data deck for the second standard test case for 3DBR-COMOC.

An extensive computational program was conducted using 3DBR-COMOC to validate use of the three-dimensional boundary region equations for this problem geometry, and to evaluate the governing influences on turbulent mixing in the three-dimensional region within the constraints of the prototype eddy viscosity model. The existence of extensive cold flow data [Ref. 23, 24] for longitudinal velocity, u_1, and hydrogen mass fraction, Y^H, provides the means to evaluate the accuracy and

consistency of the numerical predictions; the complete discussions of results is in Ref. 25. Briefly, for the first series, the experimental data at 30 diameters downstream of injection (i.e., $x_1/D = 30$) for a dynamic pressure ratio (q_r) of unity, were interpolated at the nodes of the finite element discretization, Fig. 18, using cubic spline procedures. The numerical solution was carried to $x_1/D = 60$, and the empirical constant in Eq. (67) set to $K = 0.1$ by "best" agreement with data. As shown in Fig. 19, agreement with the superimposed data along the symmetry plane, $x_3 = 0$, is excellent. Transition from mixing length to mass defect occurred between 0.6 and 1.0 injector diameters above the plate across the entire pattern. The predicted lateral spreading of the hydrogen (parallel to the x_3 axis) is in good agreement with the data spread near the wall, but is underpredicted in the mid-region of the pattern. Transition from the initial distribution, and detail on solution accuracy, are presented in Fig. 20, which compares data to computed concentration profiles along planes x_3 = constant at $x_1/D = 60$. The underpredicted lateral diffusion is prominent, stemming in part from the omission of three-dimensional influence in the

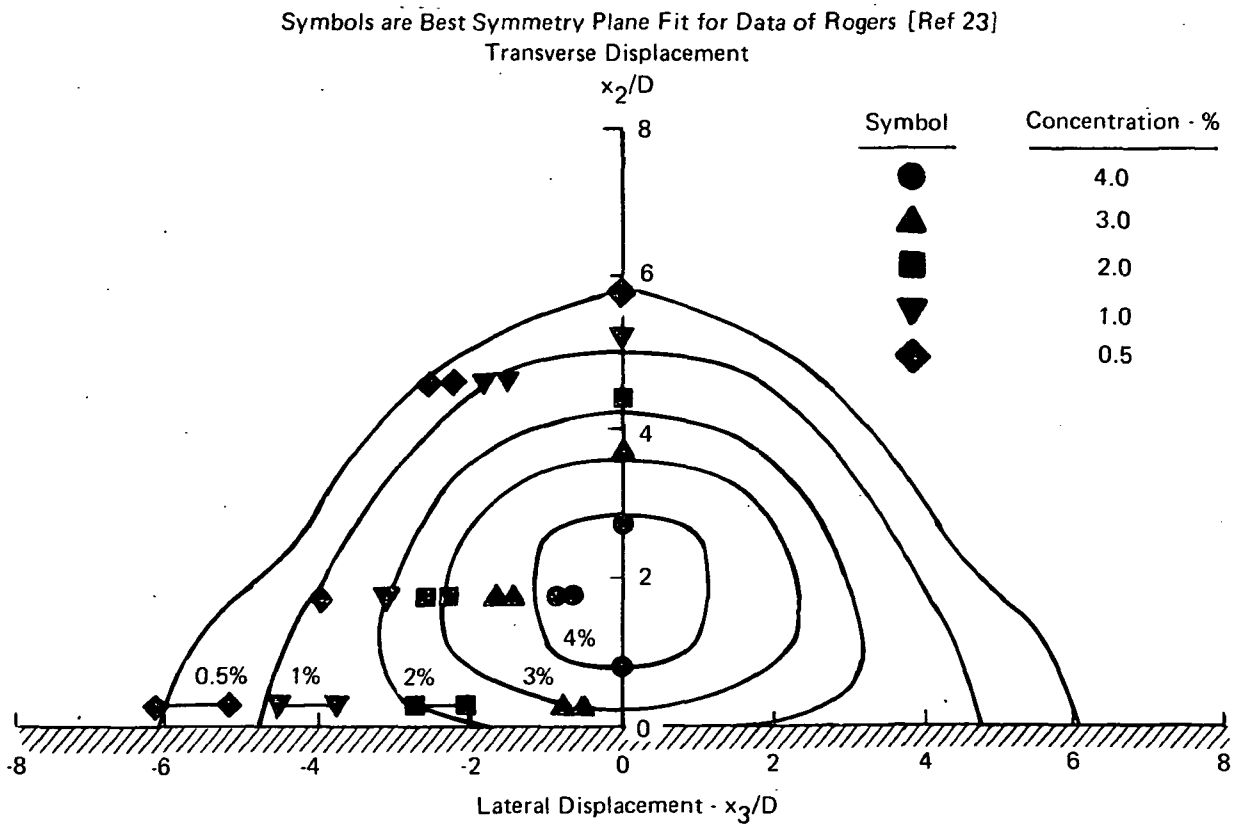

Figure 19. Computed Hydrogen Mass Fraction and Experimental Data for Single-Jet, $q_r = 1.0$, $x_1/D = 60$

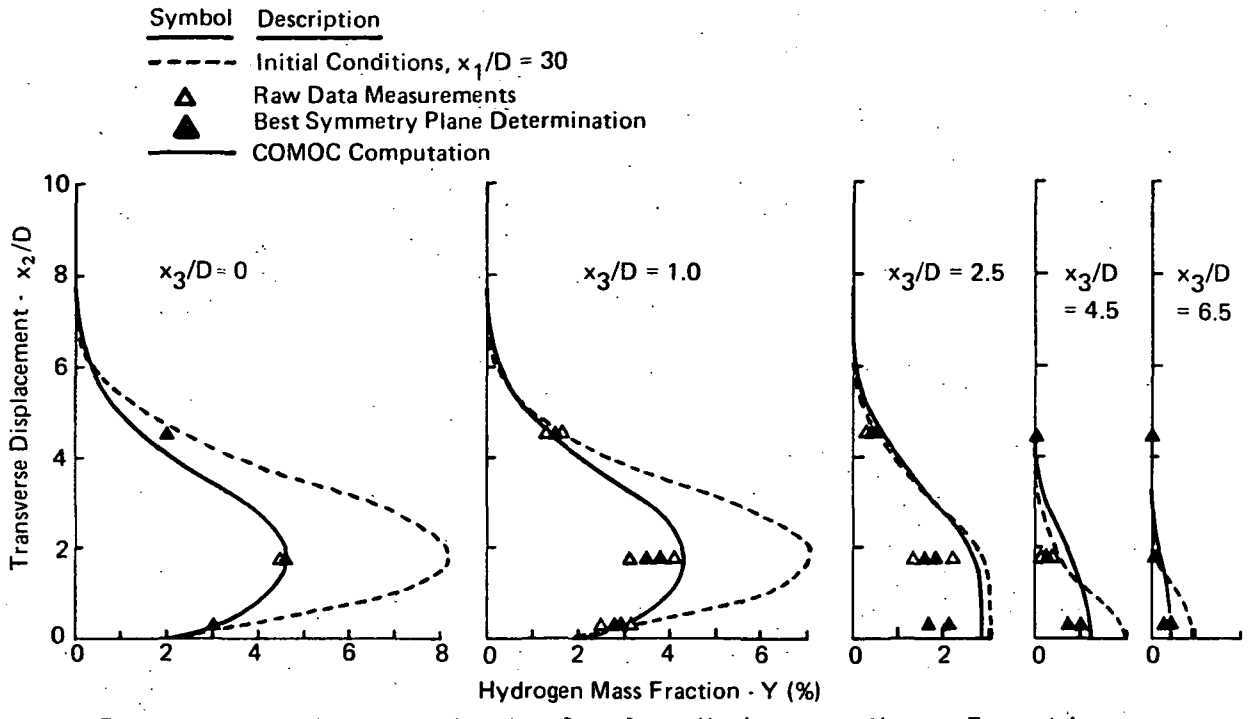

Figure 20. Computed Single-Jet Hydrogen Mass Fraction Distribution at $x_1/D = 60$, $q_r = 1.0$

turbulence model. The experimental data show that in this region, $u_{1,2}$ and $u_{1,3}$ are of equal magnitude, as observed in Fig. 21, which is a three-dimensional surface plot of the longitudinal velocity distribution at $x_1/D = 30$, as observed from a vantage point beneath the plate surface. The superimposed grid coincides with the finite element discretization (omitting diagonals), and the hydrogen jet is imbedded within the centroidal indentation. Obviously, three-dimensional effects are important, and should form an integral part of future three-dimensional turbulence modeling. Figures 22 and 23 compare the COMOC computed solutions for hydrogen mass fraction and longitudinal velocity distribution to data at $x_1/D = 120$, as well as the initial distributions. Agreement is generally quite good throughout.

This computational study was repeated using for initial conditions the experimental data for a row of orifices aligned perpendicular to the main flow vector with a uniform separation distance of 12.5 orifice diameters [Ref. 24]. For this study, the finite element discretization of Fig. 18 was simply scaled to span the symmetric half zone between ejectors, using the automatic discretizer. The vanishing normal gradient boundary condition was then applied to both lateral sides of the computational region. Shown in Fig. 24 and 25 are the COMOC computed hydrogen mass fraction profile distributions at stations $x_1/D = 60$ and $x_1/D = 120$ compared to data. Figure 26 displays the more familiar contour plot at $x_1/D = 120$. These results

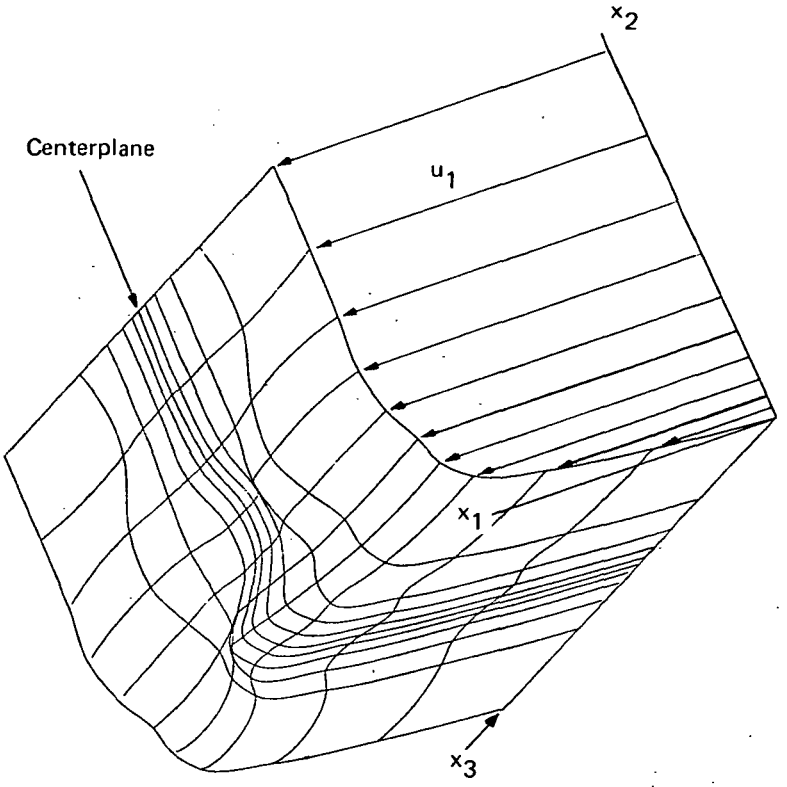

Figure 21. Isometric View of Longitudinal Velocity Surface for Single-Jet Configuration, $x_1/D = 30$

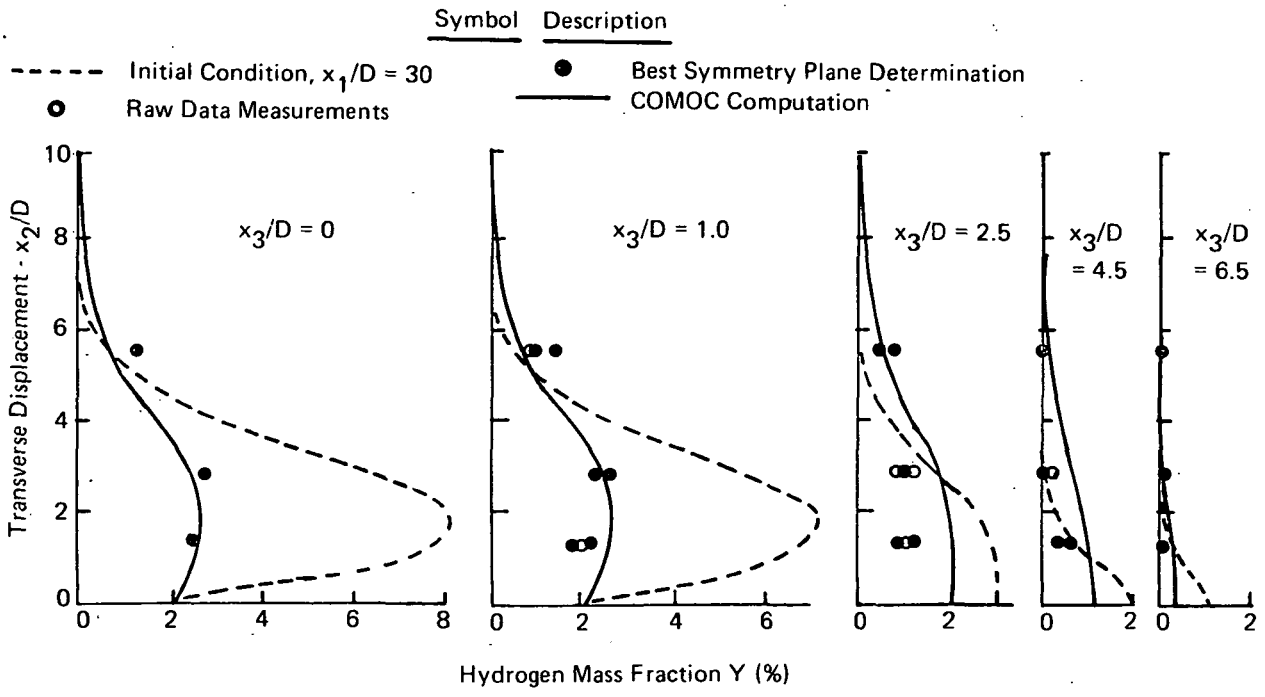

Figure 22. Computed Single-Jet Hydrogen Mass Fraction Distribution at $x_1/D = 120$, $q_r = 1.0$

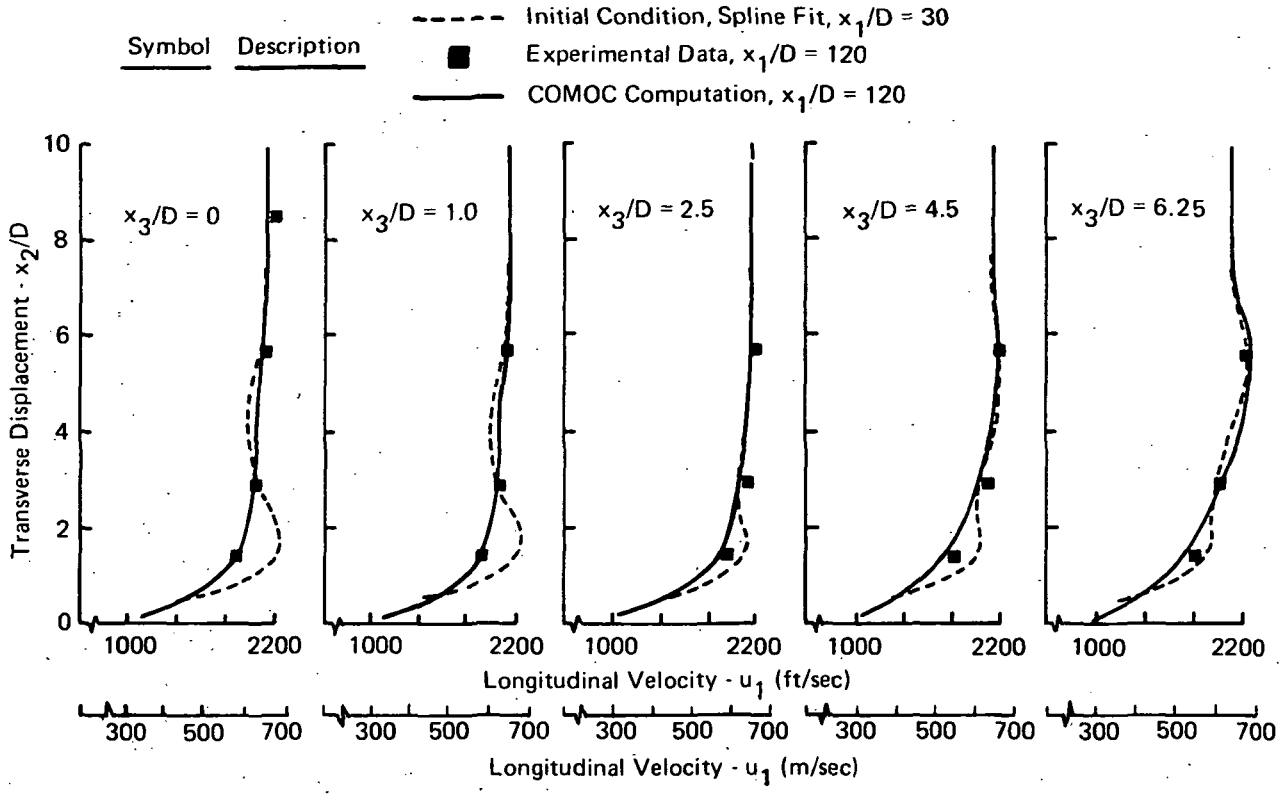

Figure 23. Computed Single-Jet Longitudinal Velocity Distribution at $x_1/D = 120$, $q_r = 1.0$

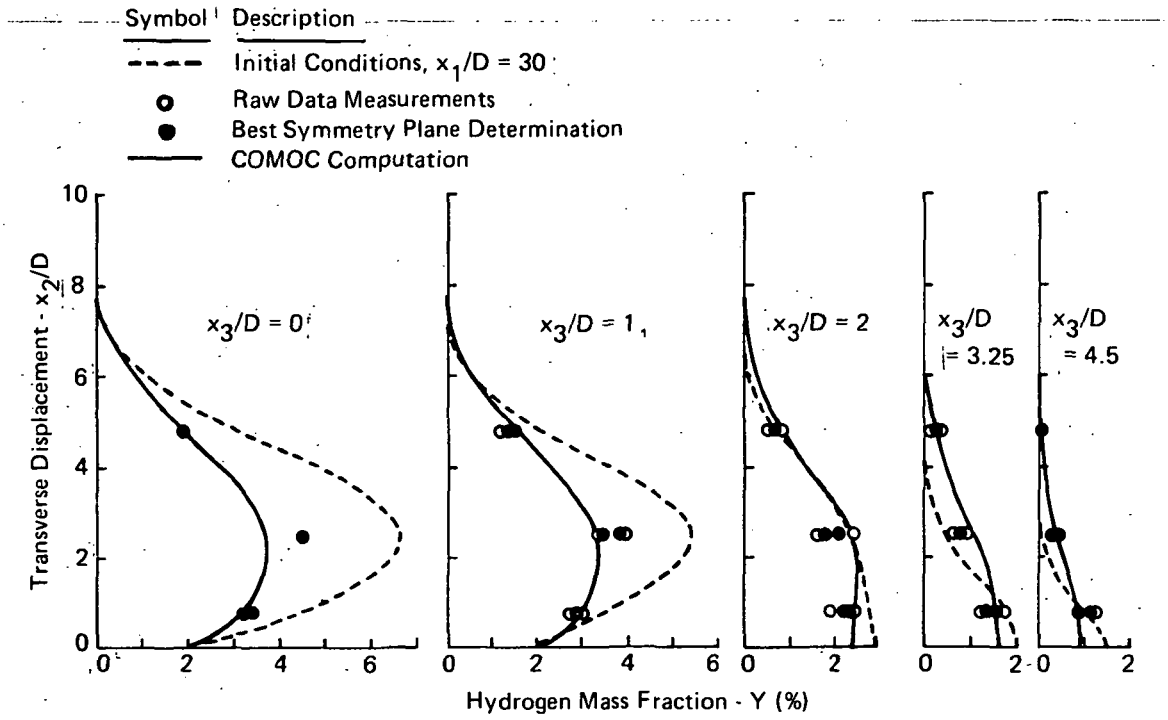

Figure 24. Computed Multijet Hydrogen Mass Fraction Distribution at $x_1/D = 60$, $q_r = 1.0$

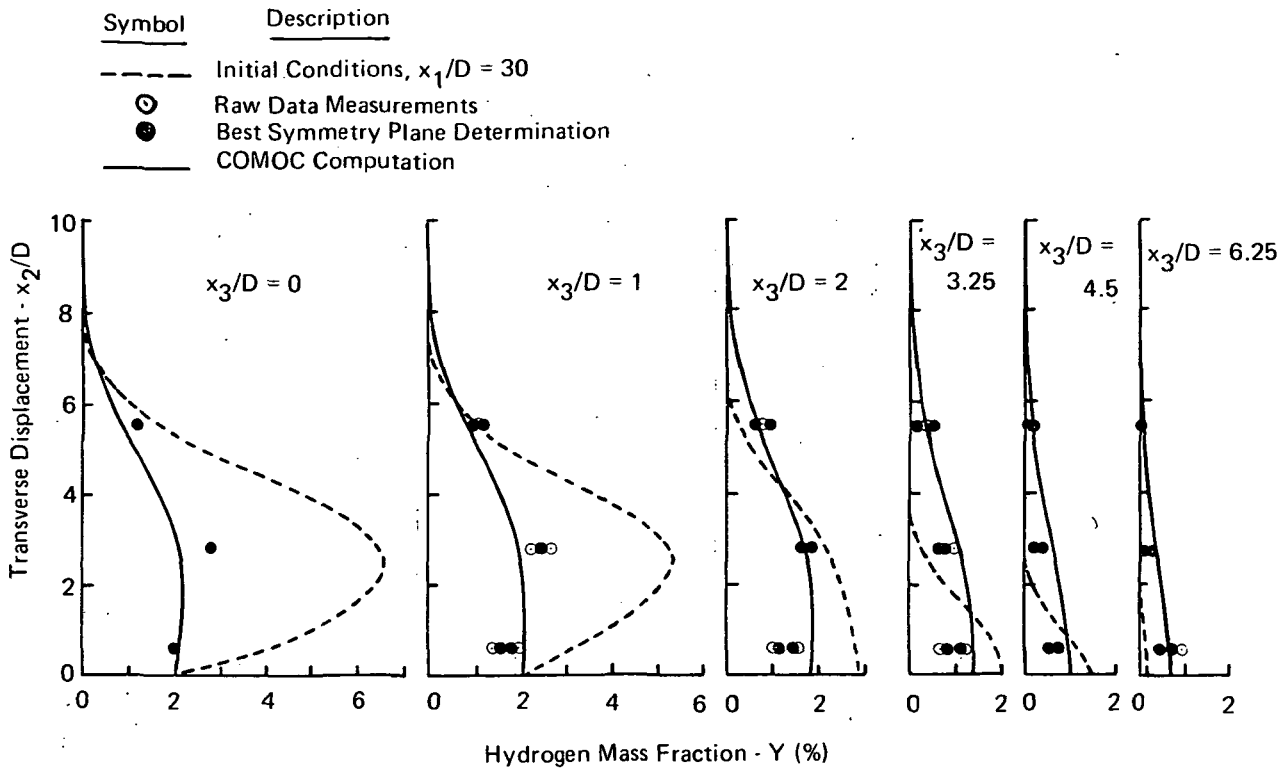

Figure 25. Computed Multijet Hydrogen Mass Fraction Distribution at $x_1/D = 120$, $q_r = 1.0$

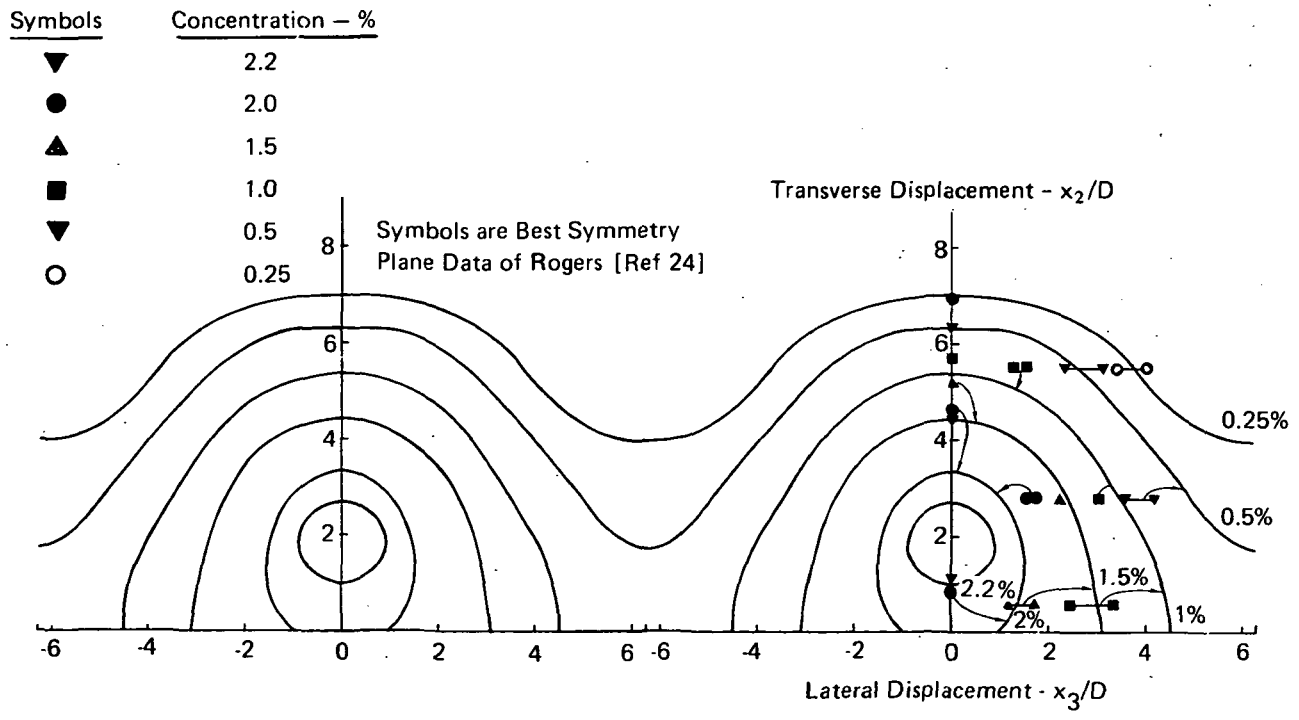

Figure 26. Computed Mass Fraction Contours and Experimental Data for Multijet, $x_1/D = 120$, $q_r = 1.0$

were obtained using the identical mixing model of the single jet, i.e., K = 0.1, Eq. (67), with transition from mixing length to mass defect occurring in the region $0.6 \leq x_2/D \leq 1.1$. Figures 24 and 25 indicate that centerplane diffusion is somewhat overpredicted, while a considerable improvement between computations and data has occurred in the lateral region. Figure 26 illustrates how the computed contour patterns merge between jets for the multiple injector configuration. Agreement between computed and measured velocity distributions at both downstream stations was excellent.

Detailed volumes of experimental data, of the type utilized to start these discussed solutions, are typically not available for complex reacting flow fields. Assuming that the foregoing studies have indeed verified the appropriateness of the differential equation system, as well as a limited validity for the turbulence model, methods for starting a three-dimensional solution with combustion are sought. One technique that shows some promise, and also admits numerical evaluation of its appropriateness, is the "virtual source." The theoretical hypothesis is simply that the complex transverse injection process can be computationally replaced by a hydrogen jet imbedded within a boundary region flow, and that the distinguishing features of this virtual source are solely dependent upon freestream and injectant parameters. The derived model [Ref. 25] captures the essence of the barrel shock-Mach disk hypothesis for injectant-freestream equilibration [Ref. 28]. To establish computational verification of this concept, the cold flow studies were repeated for the virtual source established in the plane of injection, i.e., $x_1/D = 0.0$. It was assumed to be of elliptical cross-sectional shape with the minor axis parallel to x_2, and composed of 100% hydrogen with longitudinal momentum determined from the dynamic pressure ratio, q_r. Computational evaluations of the concept were made for the three values of q_r for which data exist. Shown in Fig. 27 are typical results, obtained for virtual source simulation of the multiple injection configuration for $q_r = 1.0$. Superimposed are appropriate experimental data [Ref. 23, 24] for the key comparison bases of, 1) longitudinal trajectory of maximum hydrogen concentration, 2) height above the plate of the maximum concentration trajectory, and 3) the lateral spreading of the diffusion pattern. The peak hydrogen mass fraction is observed to drop precipitously from its initial 100% concentration, but to promptly level off in good agreement with the multijet data. The dependent variable gradients associated with this solution were quite large, yet 3DBR-COMOC maintained stable solution behavior using the automatic step-size constraint. The trajectory of the maximum hydrogen concentration above the plate surface is similarly in good agreement with multi-jet data. The computed lateral spreading agrees well with multi-jet data to $x_1/D = 30$, but is progressively underpredicted (maximum 15%) as the solution continues downstream. Similar agreement trends with data were recorded for the "softer"

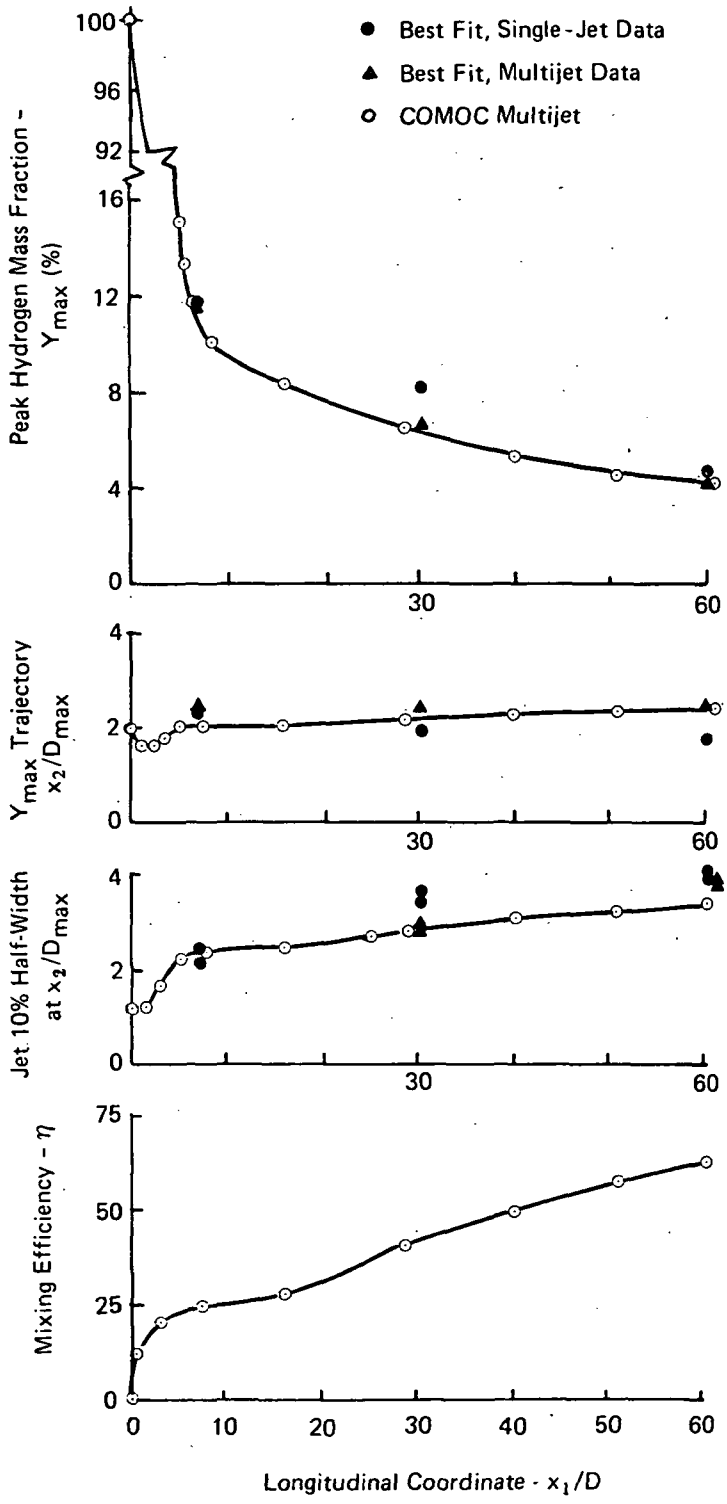

Figure 27. Prediction for Multijet Virtual Source, q_r = 1.0

injection case, q_r = 0.5. However, fairly large disparities (up to 40%) occurred for the "hard" jet, corresponding to q_r = 1.5, but for which the entire theoretical concept becomes rather suspect. Figure 27 is completed with a plot of η, an integral "mixing efficiency" parameter, [Ref. 24]. This parameter is defined as the percentage of molecular hydrogen that would be lost to the computed frozen flow H_2 mass fraction distribution if all available H_2 (or O_2, depending on the limiting reagent) was converted to H_2O within the computed velocity distribution.

The virtual source turbulent transport model was identical to the prior cold flow studies with two minor exceptions. The mixing length hypothesis, ε_1, was uniformly enforced until the minimum velocity in the virtual source depression accelerated to within ~2% of the corresponding boundary layer velocity without injection. This occurred within 8 diameters downstream of the injection plane for all q_r. Downstream of x_1/D = 8, transition from ε_1 to ε_2 occurred within one diameter above the plate surface. Due to the rather small initial density within the virtual source, the initial computed mass defect was disproportionally small. From experimentation, a smaller constant (K = 0.05) was found uniformly effective for the three studies.

With the change of one input flag, the virtual source simulation was repeated with equilibrium combustion allowed. Shown in Fig. 28 are the typical results of this computational simulation, on the multiple comparison bases previously discussed for the cold flow tests. The precipitous drop in the peak hydrogen mass fraction concentration parallels the cold flow experience, but the levels downstream of x_1/D = 7 lie well below the non-reacting experience. The trajectory of the peak hydrogen level is essentially parallel to the plate surface through x_1/D = 30. The lateral spreading of the jet is considerably more pronounced for $x_1/D>10$ in comparison to the cold flow tests. The mixing efficiency parameter, η, reaches 100% at x_1/D = 20, well ahead of the cold flow simulation. These differences reflect, in large part, the considerably different temperature and density distributions. As shown in Fig. 28, ignition occurs immediately downstream of simulated injection, and the peak temperature rapidly climbs to 2000°K (~3800°R). It remains at this level until stoichiometric mixing is completed, i.e., η = 100%; thereafter, it continuously decreases as local heat addition from combustion is unable to balance diffusion effects. A typical CPU time on the IBM 360/65 for execution of this test with combustion was about 1275 seconds. Execution of a cold flow counterpart (to x_1/D = 30) required about 950 seconds. The 325 seconds additional for combustion reflects the CPU required to execute the temperature iteration loop in the combustion subroutine for this particular test case.

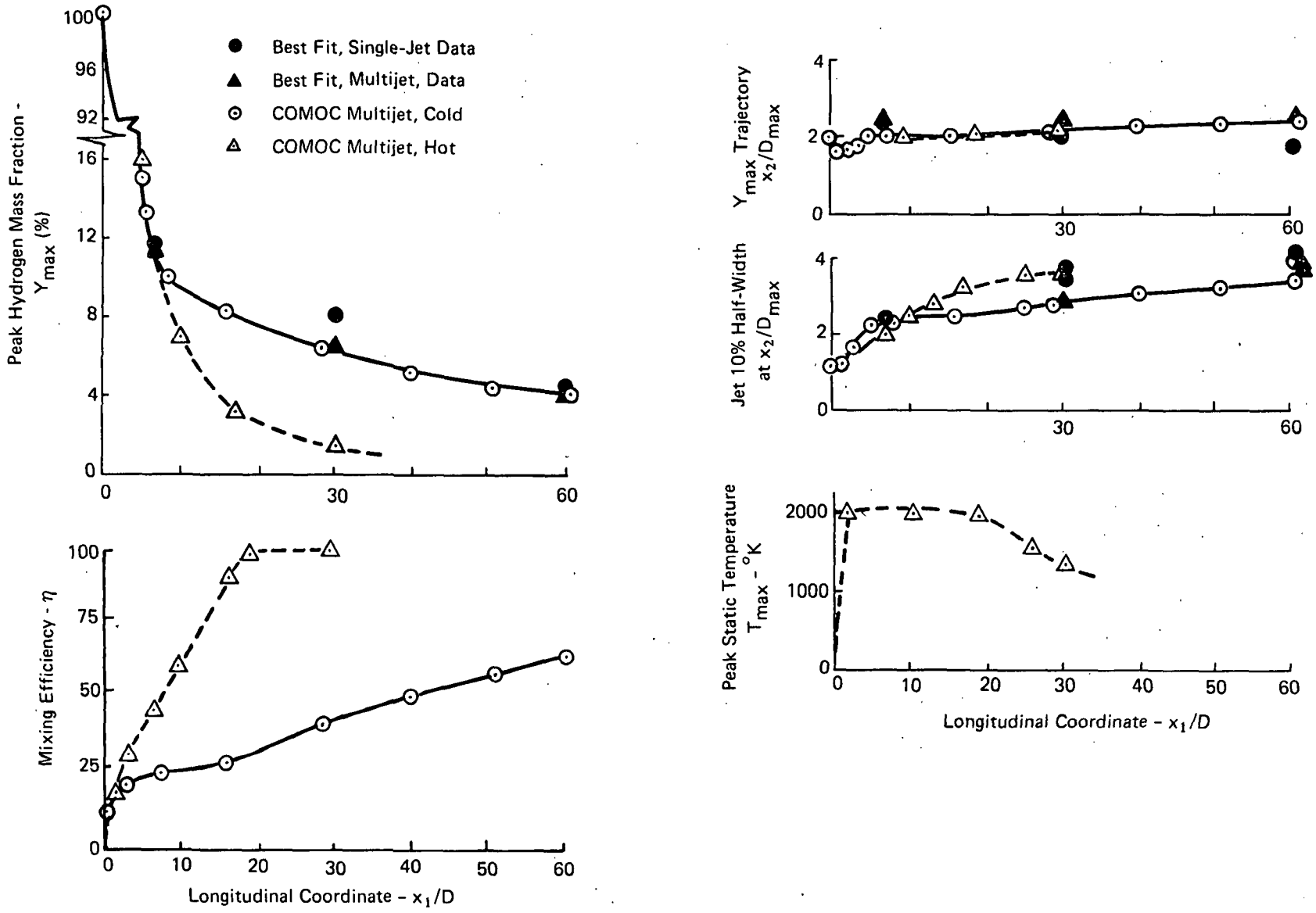

Figure 28. Prediction for Multijet Virtual Source with Equilibrium Reaction, q_r=1.0

DATA DECK PREPARATION

The data decks that generate the nominal Mach 5 isoenergetic boundary layer flow, and the three-dimensional virtual source simulation, come as standard test cases for 3DBR COMOC. The listings of these data decks are included in Appendices A and B. Another problem specification can be readily adapted from these decks, since approximately one-third of a data deck is associated with standard call sequences as well as output format specification and arrangement instructions. These standard data should not be altered without reference to the programmer's manual for 3DBR COMOC [Ref. 1]. The following discussion covers general details, and illustrative examples are pertinent to the data deck for the Mach 5 test case. Comments and descriptions should be interpreted with reference to Appendix A. Subsequently, the alterations required to establish the non-uniformly discretized virtual source problem data deck from the Mach 5 test case are presented and discussed.

Input preparation is subdivided into four phases.

Phase I. Reference Conditions and Control Parameter Specification

Call	Parameter	Code	Function
FEBL			Starts execution of COMOC
COMTITLE			Reads one title card to appear on cover page of output
FENAME			Initialization
&NAME01			Integer parameter input
	NEQKNN		Number of dependent variables to be integrated in X1 direction
	IGAS	0	Isoenergetic flow with constant c_p
		1	General flows
	IFR	0	Equilibrium composition (IGAS≡1)
		1	Frozen composition
	KDUMP	0	Suppress debug output
		1	Print debug output
	NPVSX		No. of entries in pressure table
	NSCX	0	Uniform X3 interval in discretization
		1	Non-uniform X3 interval in discretization
	NSCY	0	Uniform X2 interval in discretization
		1	Non-uniform X2 interval in discretization
&NAME02			Floating point parameter input
	UINF		Reference (freestream) velocity (F/S)
	TØFINF		Reference stagnation temperature (°R)
	REFL		Reference length (F)
	TØ		Initial X1 station (F)

Call	Parameter Code	Function
	TD	Length of X1 solution, starting at TØ (F)
	DELP	Percent of TD at which output is desired
	EPS	Integration control parameter (.01 to .0001)
	VSTART	Percent of TD at which transverse velocity (U2) computation starts
	XSCALE, YSCALE	Multipliers to convert discretization to feet
	CPA,CPH TØA,TØH XMA,XMH	Specific heats, stagnation temperatures, and molecular weights for two-component, isoenergetic, frozen flow mixing (IGAS≡0)
FEDIMN		Generate vector lengths and array entry points.

Phase II. Finite Element Discretization

LINK1 1 This call generates the finite element discretization of the X2X3 plane. The data are read in free format fields. A "T" terminates any sequence.

A. Automatic Uniform Discretization

Occurs for NSCX = NSCY = 0
Set XSCALE = desired element width in the X3 direction
Set YSCALE = desired element height in the X2 direction
Read selection keys

e.g. YSCALE = 0.004
XSCALE = 0.002
1 21, 1 2,
T

Generates discretization made up of 21 node rows × 2 node columns, or 40 elements (× 1 element). Elements are 0.004 F high by 0.002 F wide.

B. Automatic Non-Uniform Discretization

Occurs for NSCX = 1 and NSCY = 1
Set X3 discretization first, X2 discretization second. Data are used in sets of 3 integers at a time. First integer identifies finite element interval concerned, next two indicate element width (or height) as ratio in feet, e.g., 3 1200 ≡ 3/1200(F).

e.g. 1 3 1200,2 1 600,3 5 1200,...
T
1 1 600,7 1 600,8 7 1200,...
T
1 11, 1 4,
T

This generates a finite element discretization of 11 node rows × 4 node columns. The element widths (intervals between node columns) are respectively 3/1200 (F), 1/600 (F), ... The height of the first 7 element rows is uniformly 1/600 (F), eighth is 7/1200 (F), etc.

Phase III. Output Specification

Following the discretization phase, the user can input up to 10 title cards to head each generated output sequence.
The next ~65 input cards specify output format, see Appendix A, and are typically not to be changed without reference to the programmer's manual.
Up to 10 title cards can follow the standard output specification to fully describe the problem being solved. This output will occur once, directly after printing of the cover page.

DONE Calls end to output specification phase

Phase IV. Solution Parameters, Boundary Conditions, and Initial Distributions

Call	Function
VX3ST e.g. 11*I0.05 0.1	Establishes NPVSX entries into static pressure table as function of X1 Eleven pressure values at intervals ΔX1 of 0.05, starting at X1 = 0.1.
VPVSX e.g. 4.3494 3.41...	Read pressures in PSFA
IPINT -1	Standard Input consisting of integer array of numbers corresponding to dependent variables. Program will integrate first NEQKNN of them, plus U2.
KBNO (N) . . . . KBNO (NN)	KBNO (N) establishes fixed boundary conditions for dependent variables N through NN.
e.g. KBNO 4 BOTTOM DONE	Fixes variable 4 nodes on bottom of discretization at their initial input values.

Call	Function
ICALL -1 ICALLS -1 LINK3 4 LINK1 3	Fixed calling sequence for internal evaluations, not to be changed.
VTEMP -58	Read initial nodal total temperature distribution. Non-dimensionalize entries by number in location 58 (TREF).
e.g. VTEMP 82*1800. T	Read: first 82 nodes at T_o = 1800°R
VYY -(X) . . . . VYYEND (N)	Reads initial conditions for dependent variable N. Non-dimensionalize entries by number in |X|.
e.g. VYY -27 42*0.0 T VYYEND 2	Initial U2 distribution is all zeros. Non-dimensionalize entries by number in location 27 (UREF)
e.g. VYY -27 2*0.0 2*1654... .....72*4004.8 T VYYEND 1	Initial U1 distribution is zero at first two nodes, 1654 F/S at second two,..., last 72 nodes have 4004.8 F/S. Non-dimensionalize entries by number in location 27 (UREF).
QKNINT DESCRIPT DONE DESCRIPT 3 . . . . DONE COMOC END	Standard completion of data deck
EXIT	If a second test case is desired, insert data deck starting with COMTITLE before EXIT card.

Listed in Table 9 are the changes to the Mach 5 test case data deck required to establish the three-dimensional virtual source data deck. The complete listing of the latter is included as Appendix B. The following explains the alterations with respect to input phase and the line numbers in Table 9.

Input Phase	Line No.	Description
I	1	Title card for output cover page
	2	Reference condition and control parameters
	.	for combustion calculations using five
	.	dependent variables
	7	
II	8	Form non-uniform discretization, using 11
	.	node rows × 6 node columns, producing 100
	.	finite elements
	13	
III	14	Title card to head each output call
	15	Detailed problem description
	.	
	.	
	22	
IV	23	Entry locations of longitudinal pressure
	24	distribution (constant)
	25	66 nodes have uniform stagnation temperature
	26	Initial U1 distribution
	.	
	.	
	.	
	36	
	37	Initial U2 distribution is zero
	38	Initial O2 distribution reflects location of virtual source
	39	Initial N2 distribution
	40	Initial H2 distribution

Hence, establishing the data deck for a multiple dependent variable, three-dimensional problem using a non-uniform finite element discretization is readily accomplished. In this case, only forty data card changes were required, using the two-dimensional Mach 5 data deck as a master deck.

Table 9

DATA DECK CHANGES TO PRODUCE VIRTUAL SOURCE SIMULATION

Line

```
01          COMOC CHECK CASE FOR THREE DIMENSIONAL REACTING BOUNDARY REGION FLOW
02                  NEQKNN=5,           IGAS=1,             IFR=0,              KOUMP=0,
03                  NPVSX=2,            NSCX=1,             NSCY=1,
04            NE1E2=1,
05                  UINF=2272.,         TOFINF=533.0,       REFL=.003333333,
06                  TO=0.0,             TD=0.10,            DELP=5.0,           EPS=0.01,
07                  XSCALE=0.003333333, YSCALE=0.003333333, VSTART=101.0,
08            1 75  100, 2  50  100, 3  125  100, 4  150  100, 5  225  100,
09          T   INCREMENTS BETWEEN X3, NODE-NUMERATOR-DENOMINATOR
10            1  5  10, 7  5  10, 8  125  100, 9  175  100, 10  250  100,
11          T   INCREMENTS BETWEEN X2
12            1  11, 1  6,
13          T   11 ROWS AND 6 COLUMNS NORMALIZED BY LREF,HENCE X-Y SCALES =LREF
14          CHECK CASE,THREE DIMENSIONAL REACTING BOUNDARY REGION - VIRTUAL SOURCE
15          CHECK CASE,THREE DIMENSIONAL REACTING BOUNDARY REGION - VIRTUAL SOURCE
16          (H2/O2/AIR SYSTEM WITH EQUILIBRIUM CHEMISTRY). PROBLEM CONSIDERED
17          REPRESENTS TRANSVERSE H2 INJECTION INTO A SUPERSONIC AIR STREAM
18          CHARACTERISTIC OF SCRAMJET FUEL INJECTION,SEE ROGERS NASA TND-6114,
19          1971 AND NASA TND-6476,1971 FOR EXPERIMENTAL STUDY OF THIS PROBLEM.
20          TURBULENCE MODEL EMPLOYED IS DESCRIBED IN USER'S MANUAL NASA CR-132450,1974.
21          CALCULATIONS ARE STARTED USING VIRTUAL SOURCE CONCEPT TO REPLACE
22          COMPLEX NEAR INJECTION FLOW FIELD.
23           0.0     100.      T X1 TABLE FOR PRESSURE
24           193.    193.      T PRESSURE  TABLE PSF
25             66*533.
26            6*0.0
27            6*1503.
28            6*1660.
29            2*1550.   4*1759.
30            2*1550.   4*1833.
31            2*1550.   4*1892.
32            2*2272.   4*1942.
33            2*2272.   4*1985.
34            2*2272.   4*2074.
35            2*2272.   4*2169.
36            6*2272.
37            66*0.0
38           18*.233       2*0.0     4*.233     2*0.0     4*.233     2*0.0     34*.233
39           18*.767       2*0.0     4*.767     2*0.0     4*.767     2*0.0     34*.767
40           18*0.0        2*1.0     4*0.0      2*1.0     4*0.0      2*1.0     34*0.0
```

CONCLUDING REMARKS

This report documents the theoretical foundation and the mechanical structure of the Three-Dimensional Boundary Region Variant of the COMOC computer program system. A unified effort has been made to generate a computational capability that can be addressed to a wide range of problems involving complex three-dimensional flow fields without requiring undue mathematical prowess on the part of the user. The success of this type of venture can only be measured by the degree to which these goals are approached or attained. As with any large computer program, it has been debugged to the extent of the specific problems already explored. Hopefully, if bugs remain, they are not of such a debilitating nature as to severely limit the usefulness of the program. In this regard, it is suggested that the potential user first experiment with a few problems whose solution character is known, in order to attest to the program's performance for a particular problem class.

REFERENCES

1. Orzechowski, J. A. and Baker, A. J., "COMOC: Three-Dimensional Boundary Region Variant, Programmer's Manual," NASA CR-132449, 1974.

2. Baker, A. J., "Finite Element Computational Theory for Three-Dimensional Boundary Layer Flow," AIAA Paper 72-108, 1972.

3. Baker, A. J., "Finite Element Solution Algorithm for Viscous Incompressible Fluid Dynamics," Int. J. Num. Meth. Engr., 6, 1, 1973, 89-101.

4. Baker, A. J., "A Finite Element Solution Algorithm for the Navier-Stokes Equations," NASA CR-2391 , 1973.

5. Bauer, A. M. and Baker, A. J., "COMOC: Thermal Analysis Variant, User's Manual," NASA CR-130148, 1972.

6. Orzechowski, J. A., Manhardt, P. D. and Baker, A. J., "COMOC: Two-Dimensional Navier-Stokes Variant, User's Manual," Bell Aerospace Report D9198-954001, 1973.

7. Vincenti, W. G. and Kruger, C. H., Jr., Introduction to Physical Gas Dynamics, Wiley, New York, 1965.

8. Zienkiewicz, O. C., The Finite Element Method in Engineering Science, McGraw-Hill, London, 1971.

9. Nigro, B. J., "The Derivation of Optimally Stable K-Stage, One-Step Explicit Numerical Integration Methods (K = 1, 2, 3)," Bell Aerospace Report TCTN-1008, 1970.

10. Lomax, H., "On the Construction of Highly Stable, Explicit, Numerical Methods for Integrating Coupled Ordinary Differential Equations with Parasitic Eigenvalues," NASA TND-4547, 1968.

11. Nigro, B. J., "The Derivation of Optimally Stable and Accurate, 3-Stage, 1-Step, Explicit, Numerical Integration Methods," Bell Aerospace Report TCTN-1010, 1971.

12. Mascitti, V. R., "A Simplified Equilibrium Hydrocarbon-Air Combustion Gas Model for Convenient Use in Air-Breathing Engine Cycle Computer Programs," NASA L-5825.

13. Schlichting, H., Boundary Layer Theory, McGraw-Hill, New York, 1960.

14. Strang, W. G. and Fix, G. J., An Analysis of the Finite Element Method, Prentice Hall, New Jersey, 1973.

15. Baker, A. J. and Zelazny, S. W., "Predictions in Environmental Hydrodynamics Using the Finite Element Method," AIAA Paper 74-7, 1974.

16. Fischer, H. B., "Longitudinal Dispersion and Turbulent Mixing in Open Channel Flow," Annual Rev. Flu. Mech., 5, 1973, 59-78.

17. Jobson, H. E. and Sayre, W. W., J. Hyd. Div., Proceedings of ASCE, 96, 1970, 703-24.

18. Fischer, H. B., "The Effect of Bends on Dispersion in Streams," Water Resources Research, 5, 2, 1969, 496-506.

19. Patankar, S. V. and Spalding, D. B., Heat and Mass Transfer in Boundary Layers, Intertext Books, 1970.

20. Christian, J. W., Hankey, W. L. and Petty, J. S., "Similar Solutions of the Attached and Separated Compressible Laminar Boundary Layer with Heat Transfer and Pressure Gradient," ARL-70-0023, 1970.

21. Becker, J. V. and Kirkham, F. S., "Hypersonic Transports," Paper No. 25, NASA SP-292, 1971.

22. Bushnell, D., "Hypersonic Airplane Aerodynamic Technology," Paper No. 5, NASA SP-292, 1971.

23. Rogers, R. C., "A Study of the Mixing of Hydrogen Injected Normal to a Supersonic Airstream," NASA TND-6114, 1971.

24. Rogers, R. C., "Mixing of Hydrogen Injected From Multiple Injectors Normal to a Supersonic Airstream," NASA TND-6476, 1971.

25. Baker, A. J. and Zelazny, S. W., "A Theoretical Study of Mixing Downstream of Transverse Injection into a Supersonic Boundary Layer," NASA CR-112254, 1972.

26. van Driest, E. R., "On Turbulent Flow Near a Wall," J. Aero. Sci., 23, 11, 1956, 1007-1011.

27. Hinze, J. O., Turbulence, McGraw-Hill, 1959.

28. Billig, F. S., Orth, R. C. and Lasky, M., "A Unified Analysis of Gaseous Jet Penetration," AIAA J., 9, 6, 1971, 1048-1057.

APPENDIX A

DATA DECK LISTING FOR MACH 5
TWO-DIMENSIONAL FLOW CHECK CASE

```
FEBL
COMTITLE
 CHECK CASE,TWO DIMENSIONAL SUPERSONIC FLOW WITH PRESSURE GRADIENT
FENAME
 &NAME01
          NEQKNN=2,          IGAS=0,          IFR=0,          KDUMP=0,
          NPVSX=11,          NSCX=1,          NSCY=1,
 &END
 &NAME02
          UINF=4004.8,       TOFINF=1800.,    REFL=.0132
          TQ=0.1,            TD=0.2,          DELP=5.0,       EPS=.01,
          VSTART=5.0,        CPA=0.24,        CPH=3.445,      TOA=1800.,
          TOH=0.0,           XMA=28.97,       XMH=2.016,
          XSCALE=1.0,        YSCALE=1.0,
 &END
FEDIMN
LINK1    1                                                   SETUP
  1   2 1000,    2  2 1000,
  T
  1   2 1000,   21  2 1000,
  T
  1 21, 1 2,
  T
 CHECK CASE,TWO DIMENSIONAL SUPERSONIC FLOW WITH PRESSURE GRADIENT

 REFERENCE      ENGLISH-FT      ENGLISH-IN       M-K-S          C-G-S
-----------    ------------    ------------     -------        -------

DONE
MPARA   -1
   2     2    162     164     163
   2     2      2     164     163
   2     2      2     170     174
   2     2      2     165       2
   2  -175      2       2       2
   2     2      2     176       2
   2     2      2     177     178
   2     2    169     168     167
   2     2      2       2       2
   2     2    2     2

HOLIST
 LENGTH.........    .FT.........    .IN.........    .M..........    .CM.........
 VELOCITY.......    .FT/S.......    .N.A........    .M/S........    .CM/S.......
 DENSITY........    .LBM/FT3....    .N.A........    .KG/M3......    .G/CC.......
 TEMPERATURE....    .RANKINE....    .N.A........    .KELVIN.....    .N.A........
 ENTHALPY.......    .BTU/LBM....    .N.A........    .KJ/KG......    .N.A........
 FROZ.SPEC. HEAT    .BTU/LBM-R..    .N.A........    .KJ/KG-K....    .N.A........
 VISCOSITY......    .LBM/FT-S...    .N.A........    .NT-S/M2....    .POISE......
 LOCAL PRESSURE     .PSF........    .PSI........    .NT/M2......    .TORR.......
```

```
 LOCAL SOLUTION       MACH NO.        DPDX1(LBF/FT3) MAX. H2 CONC.   MIX EFF.(ETA)
 X1/LREF             DX1/LREF           EPSILON      DX1MIN/LREF
IONUMB  -1
  200     4*43     200  27   200  2*27
  200      10  200    2*10    200    58    200   58  200
  200    97  200   97  200       200  30   200   30  200
  200    38  200  2*38
 999
  200    36     36    36    36
 200
   61       100    134     122
  11    12    14    85

IOSAVE  -1
 1248  285  320  284  10248
 2248  278  4248  9248   8248
 1247  334   292  314
 T U,T,HS,RHO,N2,V,CP,HTOT,H2,O2,DIFU,PR NO.,LAM.VISC.,SCT.NO.
IOMULT  -1
 14*2
 T U,T,HS,RHO,N2,V,CP,HTOT,H2,O2,DIFU,PR NO.,LAM.VISC.,SCT.NO.
DESCRIPT 2
U1/UREF          T/TREF           HSTAT/HREF       RHO/RHOREF       ELEM.N2 MAS.FRAC
U2/UREF          CPF/CPFREF       HTOT/HREF        ELEM.H2 MAS.FRACELEM.O2 MAS.FRAC
EFF.MU/MUREF     EFF. PRANDTL NO.MU/MUREF          EFF.SCHMIDT NO.
COMOC
DESCRIPT
  COMOC CHECK CASE FOR TWO-DIMENSIONAL FLOW WITH PRESSURE GRADIENT.
 A COMPARABLE SIMILARITY SOLUTION HAS BEEN REPORTED BY CHRISTIAN ET AL,
 ARL 70-0023. SPECIFIC CASE CONSIDERED CORRESPONDS TO MACH NO.5 BETA=0.5,
 S(0)=0 (ADIABATIC WALL). SOLUTION STARTED AT X=0.10 FT. WITH SIMILAR
 SOLUTION PROFILE.LAMINAR FLOW WITH VISCOSITY FROM SUTHERLANDS LAW.
 DISCRETIZATION SPANS THREE TIMES INITIAL BOUNDARY LAYER THICKNESS.
 ISOENERGETIC FLOW WITH TOTAL TEMPERATURE = 1800 R.
DONE
VX3ST
    11*10.05  0.1                        T  X1 TABLE FOR PRESSURE
VPVSX
  4.3494  3.41  2.846  2.46  2.2176  2.02  1.857  1.73  1.6178  1.53  1.4451
 T
IPINT   -1
    1    4    8   10    9    3    2  T INTEGRATE U1,ENTH.,O2,N2,H2,U3,U2
KBNO    1
BOTTOM              DONE
        FIXES U1 (VARIABLE NO. 1) ALONG WALL TO INITIAL VALUE
KBNO    2
BOTTOM              DONE
        FIXES U2 (VARIABLE NO. 2) ALONG WALL TO INITIAL VALUE
KBNO    4
BOTTOM              DONE
```

```
        FIXES H  (VARIABLE NO. 4) ALONG WALL TO INITIAL VALUE
ICALL   -1
    2    5    2    2  1 1  2  T
ICALLS  -1
   10    6    4   12  5 6  3  T
LINK3    4                                                          DIMEN
LINK1    3                                                          GEOMFL
VTEMP                        -58
    42*1800.
 T  INITIAL TOTAL TEMPERATURE PROFILE
VYY                     -27
 2*0.0  2*865.    2*1654.   2*2373.   2*3004.   2*3550.   2*3879.
        2*3992.   2*4CC4.2           24*4004.8
 T  INITIAL U1 PROFILE
VYYEND   1
VYY                     -27
   2*0.0     2*2.12    2*20.14   2*53.52   2*83.2    2*109.3   2*165.
   2*253.    2*447.    24*45C.
 T  INITIAL U2 PROFILE
VYYEND   2
VYY
           42*.2330
 T INITIAL O2 MASS FRACTION PROFILE
VYYEND   8
VYY
           42*.767C
 T INITIAL N2 MASS FRACTICN PROFILE
VYYEND  10
VYY
           42*0.C
 T INITIAL H2 MASS FRACTICN PROFILE
VYYEND   9
OKNINT
DESCRIPT
DONE
DESCRIPT 3
 REFERENCE LENGTH,LREF                              43 FT.
 REFERENCE VISCOSITY,LAMINAR VALUE
 EVALUATED AT REF. TEMPERATURE.                     38 LBM/FT-S
 FREESTREAM VELOCITY AT XO(=UREF)                   27 FT/S
 STAGNATION TEMPERATURE (CONSTANT,=TREF)            58 DEG R
 FREESTREAM DENSITY AT XO(=RHOREF)                  10 LBM/FT3
 FREESTREAM MACH NUMBER AT XO                      154
 STATIC PRESSURE AT XC                               9 PSF
 NUMBER OF NODES                                   -16
 NUMBER OF FINITE ELEMENTS                         -14
DONE
COMOC
END
EXIT
```

APPENDIX B

DATA DECK LISTING FOR VIRTUAL SOURCE THREE-DIMENSIONAL CHECK CASE

```
FEBL
COMTITLE
  COMOC CHECK CASE FOR THREE DIMENSIONAL REACTING BOUNDARY REGION FLOW
FENAME
 &NAMEO1
          NEQKNN=5,          IGAS=1,          IFR=0,          KDUMP=0,
          NPVSX=2,           NSCX=1,          NSCY=1,
    NE1E2=1,
 &END
 &NAMEO2
          UINF=2272.,        TCFINF=533.0,    REFL=.003333333,
          TO=0.0,            TD=0.10,         DELP=5.0,       EPS=0.01,
          XSCALE=C.003333333, YSCALE=0.003333333, VSTART=101.0,
 &END
FEDIMN
LINK1    1                                                    SETUP
    1 75  100, 2  50  100, 3  125  100, 4  150  100, 5  225  100,
T   INCREMENTS BETWEEN X3, NODE-NUMERATOR-DENOMINATOR
    1  5  10, 7  5  10, 8  125  100, 9  175  100, 10  250  100,
T   INCREMENTS BETWEEN X2
    1  11, 1  6,
T   11 ROWS AND 6 COLUMNS NORMALIZED BY LREF,HENCE X-Y SCALES =LREF
  CHECK CASE,THREE DIMENSIONAL REACTING BOUNDARY REGION - VIRTUAL SOURCE

 REFERENCE      ENGLISH-FT      ENGLISH-IN       M-K-S           C-G-S
-----------    ------------    ------------     -------         -------

DONE
MPARA   -1
    2     2    162     164     163
    2     2      2     164     163
    2     2      2     170     174
    2     2      2     165       2
    2  -175      2       2       2
    2     2      2       176     2
    2     2      2     177       178
    2     2    169     168     167
    2     2        2       2     2
    2     2    2     2

HOLIST
 LENGTH.........    .FT.........    .IN.........    .M..........    .CM.........
 VELOCITY.......    .FT/S.......    .N.A........    .M/S........    .CM/S.......
 DENSITY........    .LBM/FT3....    .N.A........    .KG/M3......    .G/CC.......
 TEMPERATURE....    .RANKINE....    .N.A........    .KELVIN.....    .N.A........
 ENTHALPY.......    .BTU/LBM....    .N.A........    .KJ/KG......    .N.A........
 FROZ.SPEC. HEAT    .BTU/LBM-R..    .N.A........    .KJ/KG-K....    .N.A........
 VISCOSITY......    .LBM/FT-S...    .N.A........    .NT-S/M2....    .POISE......
 LOCAL PRESSURE     .PSF........    .PSI........    .NT/M2......    .TORR.......
 LOCAL SOLUTION      MACH NO.      DPDX1(LBF/FT3)  MAX. H2 CONC.   MIX EFF.(ETA)
```

```
 X1/LREF              DX1/LREF              EPSILON      DX1MIN/LREF
IONUMB  -1
  200     4*43     200  27   200  2*27
  200      10  200    2*10    200    58    200   58  200
  200    97  200  97  200       200  30   200   30  200
  200    38  200  2*38
 999
  200    36     36    36    36
 200
    61       100    134     122
  11    12    14    85

IOSAVE  -1
 1248  285  320  284  10248
 2248  278  4248  9248   8248
 1247  334   252  314
 T U,T,HS,RHO,N2,V,CP,HTOT,H2,O2,DIFU,PR NO.,LAM.VISC.,SCT.NO.
IOMULT  -1
 14*2
 T U,T,HS,RHO,N2,V,CP,HTOT,H2,O2,DIFU,PR NO.,LAM.VISC.,SCT.NO.
DESCRIPT 2
U1/UREF          T/TREF          HSTAT/HREF      RHO/RHOREF      ELEM.N2 MAS.FRAC
U2/UREF          CPF/CPFREF      HTOT/HREF       ELEM.H2 MAS.FRACELEM.O2 MAS.FRAC
EFF.MU/MUREF     EFF. PRANDTL NO.MU/MUREF        EFF.SCHMIDT NO.
COMOC
DESCRIPT
  CHECK CASE,THREE DIMENSIONAL REACTING BOUNDARY REGION - VIRTUAL SOURCE
  (H2/O2/AIR SYSTEM WITH EQUILIBRIUM CHEMISTRY). PROBLEM CONSIDERED
  REPRESENTS TRANSVERSE H2 INJECTION INTO A SUPERSONIC AIR STREAM
  CHARACTERISTIC OF SCRAMJET FUEL INJECTION,SEE ROGERS NASA TND-6114,
  1971 AND NASA TND-6476,1971 FOR EXPERIMENTAL STUDY OF THIS PROBLEM.
  TURBULENCE MODEL EMPLOYED IS DESCRIBED IN USER'S MANUAL NASA CR-132450,1974.
  CALCULATIONS ARE STARTED USING VIRTUAL SOURCE CONCEPT TO REPLACE
  COMPLEX NEAR INJECTION FLOW FIELD.
DONE
VX3ST
   0.0      100.      T X1 TABLE FOR PRESSURE
VPVSX
   193.     193.      T PRESSURE  TABLE PSF
IPINT   -1
    1    4    8   10    9    3    2  T INTEGRATE U1,ENTH.,O2,N2,H2,U3,U2
KBNO    1
BOTTOM              DONE
        FIXES U1 (VARIABLE NO. 1) ALONG WALL TO INITIAL VALUE
KBNO    2
BOTTOM              DONE
        FIXES U2 (VARIABLE NO. 2) ALONG WALL TO INITIAL VALUE
KBNO    4
BOTTOM             3DONE
        FIXES H  (VARIABLE NO. 4) ALONG WALL TO INITIAL VALUE
```

```
KBNO      8
BOTTOM                3DONE
          FIXES H  (VARIABLE NO. 8) ALONG WALL TO INITIAL VALUE
KBNO      9
BOTTOM                3DONE
          FIXES H  (VARIABLE NO. 9) ALONG WALL TO INITIAL VALUE
KBNO     10
BOTTOM                3DONE
          FIXES H  (VARIABLE NO. 10 ALONG WALL TO INITIAL VALUE
ICALL    -1
     2    5     2     2  1 1  2  T
ICALLS   -1
    10    6     4    12  5 6  3  T
LINK3     4                                                          DIMEN
LINK1     3                                                          GEOMFL
VTEMP                          -58
      66*533.
 T  INITIAL TOTAL TEMPERATURE PROFILE
VYY                      -27
     6*0.0
     6*1503.
     6*1660.
     2*1550.    4*1759.
     2*1550.    4*1833.
     2*1550.    4*1892.
     2*2272.    4*1942.
     2*2272.    4*1985.
     2*2272.    4*2074.
     2*2272.    4*2169.
     6*2272.
 T  INITIAL U1 PROFILE
VYYEND    1
VYY                      -27
     66*0.0
 T  INITIAL U2 PROFILE
VYYEND    2
VYY
    18*.233         2*0.0      4*.233     2*0.0      4*.233     2*0.0      34*.233
 T  INITIAL O2 MASS FRACTION PROFILE
VYYEND    8
VYY
    18*.767         2*0.0      4*.767     2*0.0      4*.767     2*0.0      34*.767
 T  INITIAL N2 MASS FRACTION PROFILE
VYYEND   10
VYY
    18*0.0          2*1.0      4*0.0      2*1.0      4*0.0      2*1.0      34*0.0
 T  INITIAL H2 MASS FRACTION PROFILE
VYYEND    9
QKNINT
DESCRIPT
DONE
DESCRIPT 3
 REFERENCE LENGTH,LREF                                  43 FT.
 REFERENCE VISCOSITY.LAMINAR VALUE
 EVALUATED AT REF. TEMPERATURE.                         38 LBM/FT-S
 FREESTREAM VELOCITY AT XC(=UREF)                       27 FT/S
 STAGNATION TEMPERATURE (CONSTANT,=TREF)                58 DEG R
 FREESTREAM DENSITY AT XO(=RHOREF)                      10 LBM/FT3
 FREESTREAM MACH NUMBER AT XO                          154
 STATIC PRESSURE AT XC                                   9 PSF
 NUMBER OF NODES                                       -16
 NUMBER OF FINITE ELEMENTS                             -14
DONE
END
EXIT
```